**Kaunas University of Technology**

Faculty of Mathematics and Natural Sciences

# $TiO_2$ Antibacterial Films

Master's Final Project

---

Project prepared by

**Ugnė Lapienė**

Project supervisor

**Assoc. prof. dr. Kristina Bočkutė**

---

**Kaunas, 2026**

**Kaunas University of Technology**
Faculty of Mathematics and Natural Sciences

# $TiO_2$ Antibacterial Films

Master's studies final project
Medical Physics, code 6213GX001

Project prepared by
**Ugnė Lapienė**

Project supervisor
**Assoc. prof. Dr. Kristina Bočkutė**

Project reviewed by
**Assoc. prof. Dr. Jurgita Čyvienė**

**Kaunas, 2026**

**Kaunas University of Technology**

Faculty of Mathematics and Natural Sciences

Ugnė Lapienė

# $TiO_2$ ANTIBACTERIAL FILMS

## Declaration of academic integrity

I confirm that:

1. I have prepared this final project independently and honestly, without violating the copyright or other rights of other persons, in compliance with the Law on Copyright and Related Rights of the Republic of Lithuania, the provisions of Kaunas University of Technology (hereinafter referred to as the University) on the management and transfer of intellectual property, and the ethical requirements set out in the University's Code of Academic Ethics;

2. All data and research results presented in the final project are accurate and obtained legally, no part of the project has been plagiarized from printed or electronic sources, and all quotations and references presented in the text of the final project are indicated in the list of references;

3. I have complied with personal data protection requirements in the final project, have not used undisclosed or confidential data without legal grounds, and if I have used such data, it has been properly anonymized;

4. If I used artificial intelligence (hereinafter referred to as AI) or other automated tools in preparing the final project, I applied them in accordance with the procedures established by the University, without violating the principles of academic integrity.

5. I have not paid and am not obliged to pay any sum of money not provided for by law for the final project or any part thereof to any natural or legal person;

6. I understand that if academic dishonesty or violation of other persons' rights is discovered, I will be held accountable in accordance with the procedures established by the University and may be expelled from the University; cases of academic dishonesty may be investigated even after graduation, initiating the procedure for revoking the degree.

Lapienė Ugnė. $TiO_2$ antibacterial films. Master's final project / project supervised by doc. dr. Kristina Bočkutė; Kaunas University of Technology, Mathematics and Natural Sciences faculty.

Field of study and group of fields of study: Medical Technologies (Health Sciences)

Keywords: $TiO_2$, antibacterial thin films, UV, AgNP/silver nanoparticles, *Bacillus subtilis*

Kaunas, 2026. 46 p.

## Summary

Healthcare-associated infections driven by resilient, spore-forming pathogens present a severe challenge for clinical sterilization protocols. Photocatalytic semiconductor coatings, particularly titanium dioxide ($TiO_2$) doped with noble metals, offer a promising solution via the generation of reactive oxygen species (ROS) and localized antimicrobial effects, such as cytotoxic ion release. Analysis of the fabrication and microbial evaluation of anatase $TiO_2$ thin films modified with silver nanoparticles (AgNPs) yielded critical flaws in current antimicrobial study methodology.

$TiO_2$ films were deposited using direct current (DC) magnetron sputtering and annealed to stabilize the anatase phase. Nanoparticle modification was achieved by depositing silver layers (5 nm, 7.5 nm and 10 nm) via radiofrequency (RF) magnetron sputtering, followed by solid-state dewetting at 400 °C. Surfaces were characterized using optical microscopy and water contact angle measurements. Antibacterial efficacy against *B. subtilis* was evaluated by adapting ISO 27447:2019 film cover method.

Water contact angle measurements revealed highly hydrophilic films, from baseline 57.44° ($TiO_2$) to approximately 1° (10 nm Ag). Microbiological testing yielded zero colony growth across all irradiated samples when using saline or 1/500 Nutrient Broth (NB) as washout liquid. The modified ISO 27447:2019 protocol did not take into consideration the production of EPS by bacteria. Methylene blue staining confirmed the presence of bacterial spores on the films post washing. XDLVO simulations demonstrated $TiO_2$ and AgNP/$TiO_2$ film interactions with *B. subtilis* bacteria. Investigations with $TiO_2$ showed that anatase remains inert under both dark and UV conditions, while AgNP/$TiO_2$ films showed a reduction in the bacterial population based on silver concentration. The simulation failed to consider biological factors of bacterial interactions, which overpower electrostatic interactions of $TiO_2$ thin films. Bright-field and dark-field microscopy confirmed the degradation of AgNP/$TiO_2$ film surface morphology post-experimentation. Mechanical forces required to detach EPS compounds compromise structural integrity, potentially leading to release of cytotoxic $Ag^+$ ions into post-wash bacterial suspension.

Lapienė Ugnė. $TiO_2$ antibakterinės dangos. Magistro baigiamasis projektas / vadovas doc. Dr. Kristina Bočkutė; Matematikos ir gamtos mokslų fakultetas, Kauno technologijos universitetas.

Studijų kryptis ir sritis (studijų krypčių grupė): Medicinos technologijos (Sveikatos mokslai)

Reikšminiai žodžiai: $TiO_2$, antibakterinės dangos, ultravioletinė spinduliuotė, AgNP, *Bacillus subtilis*

Kaunas, 2026. 46 p.

**Santrauka**

Sveikatos priežiūros įstaigose plintančios infekcijos, kurias sukelia atsparūs, sporas formuojantys patogenai, kelia rimtų iššūkių klinikinės sterilizacijos protokolams. Fotokatalitinės puslaidininkių dangos, ypač titano dioksidas ($TiO_2$), padengtas tauriaisiais metalais, suteikia sprendimą pasitelkiant reaktyvių deguonies formų (ROS) generavimo ir citotoksinių jonų išsiskyrimu. Anatazo fazės $TiO_2$ plonų sluoksnių, modifikuotų sidabro nanodalelėms (AgNPs), gamybos ir antimikrobinio vertinimo analizė atskleidė esminių trūkumų dabartinėje antimikrobinių tyrimų metodikoje.

$TiO_2$ sluoksniai buvo fabrikuoti naudojant nuolatinės srovės (DC) magnetroninį dulkinimą ir atkaitinti, kad būtų stabilizuota anatazo fazė. Nanodalelių modifikacija buvo atlikta užnešant sidabro sluoksnius (5 nm, 7.5 nm, 10 nm) po kurio sekė kieto kūno sudrėkinimas (angl. *solid-state dewetting*) 400 °C temperatūroje. Paviršiai buvo tirti naudojant optinę mikroskopiją ir vandens kontaktinio kampo matavimus. Antibakterinis efektyvumas prieš *B. subtilis* buvo įvertintas pritaikius ISO 27447:2019 plėvelės dengimo metodą.

Vandens kontaktinio kampo matavimai parodė itin hidrofilinius sluoksnius, nuo pradinio 57.44° ($TiO_2$) iki apie 1° (10 nm Ag). Mikrobiologiniai tyrimai parodė kolonijų neaugimą visuose mėginiuose, kai plovimui buvo naudojamas fiziologinis tirpalas arba 1/500 maistinis sultinys (NB). Modifikuotas ISO 27447:2019 protokolas neatsižvelgė į bakterijų gaminamas ekstraląstelines polimerines medžiagas (EPS). Ląstelių dažymas metileno mėlynuoju tirpalu patvirtino bakterinių sporų buvimą ant dangų. XDLVO modeliavimai demonstravo $TiO_2$ ir AgNP/$TiO_2$ sluoksnių sąveiką su *B. subtilis* bakterijomis. Modeliavimas parodė, kad anatazas išlieka inertiškas tiek UV, tiek tamsos sąlygomis, tuo tarpu AgNP/$TiO_2$ dangos parodė bakterijų populiacijos sumažėjimą priklausomai nuo sidarbo koncentracijos. Modeliuojant nepavyko įvertinti biologinių bakterijų sąveikos veiksnių, kurie įveikia $TiO_2$ plonų sluoksnių elektrostatines sąveikas. Šviesiojo ir tamsiojo lauko mikroskopija patvirtino AgNP/$TiO_2$ dangų paviršiaus morfologinę degradaciją po eksperimento. Mechaninės jėgos, reikalingos EPS junginiams atskirti nuo dangų, pažeidžia struktūrinį vientisumą, o tai gali lemti $Ag^+$ jonų išsiskyrimą į bakterijų suspensiją po plovimo.

## Contents

## List of figures

## List of abbreviations and terms

AB – Lewis acid-base interaction
AgNPs – silver nanoparticles
CAUTI – catheter-associated urinary tract infections
CFU – colony-forming unit
DAIs – device-associated infections
DLVO – Derjaguin-Landau-Verwey-Overbeek theory
EL – electrostatic interaction
EPS – extracellular polymeric substances
HAIs – healthcare-associated infections
LED – light-emitting diode
LSPR – localized surface plasmon resonance
LW – Lifshitz-van der Waals interaction
OD – optical density
ROS – reactive oxygen species
RPM – rotations-per-minute
UV – ultraviolet light
VAP – ventilator-associated pneumonia
XDLVO – extended Derjaguin-Landau-Verwey-Overbeek theory

## Introduction

Healthcare-associated infections (HAIs) are an exponentially growing problem and a critical challenge to global patient safety in modern healthcare systems. These infections, often acquired 48 or more hours after hospital admission, are a significant contributor to patient mortality, morbidity and overall longer hospital stays [1–3]. HAIs are a disproportionately more prevalent in lower- and middle-income communities, where the incidence of infection spread in hospitals can be two to ten times higher than in high-income countries [1]. For example, prevalence of catheter-associated urinary tract infections (CAUTI) can be as high as 43.28 % in low-resource countries, contributing to a higher mortality rate [2]. This disparity is due to the lack of trained personnel, lack of surveillance and limited availability of specialized sterilization equipment [4].

Main causes of HAIs remain post-surgical bacterial contamination at the operation site, catheterization and long-term use of implanted prosthetics [3]. Incidence of illness due to microorganisms is more frequent in the Intensive Care Unit, as the patients require extended medical care and invasive medical devices to maintain regular bodily functions [2,3]. Devices, such as ventilators for respiration and catheters for urinary draining, create entry points for microorganisms, promoting the spread of device-associated infections (DAIs). DAIs, such as central line-associated bloodstream infections, ventilator-associated pneumonia (VAP) or the previously mentioned CAUTI, can be lethal and overall contribute to antibiotic consumption [1].

The management and care required for HAIs is complicated by the emergence and rapid growth of antibiotic resistance [4]. The reliance on broad-spectrum antibiotics has yielded many multidrug-resistant microorganisms, leading to a shortage of effective pharmaceutical treatment options for infections [5]. Bacteria, such as *Bacillus subtilis*, while often classified and regarded as non-pathogenic, serve as vital models for studying resistance to antibiotics and sterilization techniques due to their ability to form complex and durable biofilms. These biofilms act as shields, protecting the bacterial colonies from physical and chemical threats, such as the host immune system and external antibiotics [6].

To transition from chemical treatments, researchers are turning toward self-cleaning semiconductor coatings. Titanium dioxide ($TiO_2$) is a great candidate for such coatings due to its biocompatibility and the ability to generate Reactive Oxygen Species (ROS) under UV irradiation, which destroys bacterial cells. To enhance this effect, the incorporation of silver (Ag) into the structure of the thin film coating as a co-catalyst has shown promise. Silver acts as a secondary biocide and prevents electron-hole recombination in the $TiO_2$, extending its effectiveness into the visible light spectrum and increasing overall efficacy [7].

However, the effectiveness of these films relies heavily on manufacturing parameters, such as annealing temperature and concentration of metals. Additionally, the physical interaction between the bacteria and the film remains poorly understood in experimental verification.

The aim of this work is to investigate the antibacterial effectiveness of $TiO_2$ thin films modified with silver nanoparticles (AgNPs) against *Bacillus subtilis*, utilizing microbiological testing and computational modelling.

The objectives for this work were:

1. To computationally simulate the interaction forces and antibacterial potential of $TiO_2$/AgNP thin films using XDLVO theory.

2. To adapt and validate an experimental protocol for evaluating the antibacterial efficacy of $TiO_2$/AgNP films against *B. subtilis*.

3. To evaluate the structural characteristics, integrity and stability of $TiO_2$/AgNP films used for antibacterial purposes.

# 1. Literature Review

## 1.1. Titanium dioxide ($TiO_2$) as a photocatalyst

### 1.1.1. Applications of titanium dioxide

As a semiconductor oxide, titanium dioxide ($TiO_2$) has a broad spectrum of technological applications. Its prominence in various fields of research can be credited to its high photocatalytic activity, chemical stability, cost-effectiveness and biocompability [8–10]. These properties, coupled with a favorable bandgap energy, particularly in the anatase phase, make it a great candidate for its utilization in photovoltaics and solar cells for energy conversion [8,11].

Beyond its use in the energy sector, $TiO_2$ is also widely utilized in environmental remediation to mitigate the accumulation of persistent organic pollutants in ecosystems [12]. By being able to initiate advanced oxidation processes, it photogenerates hydroxyl radicals (·OH) capable of mineralizing complex organic structures. This is vital for degrading compounds such as synthetic dyes, toxic pesticides and pharmaceuticals, that conventional water treatments cannot eliminate [12,13]. Furthermore, the high oxidative potential of $TiO_2$ facilitates photo-electrochemical water splitting. First described in 1972 by Fujishima and Honda, the process can be described as absorbed light energy generating electron-hole pairs ($e^-$ / $h^+$), triggering reduction-oxidation reactions that dissociate water molecules. Water molecules get oxidized by the holes, resulting in the production of oxygen, while the electrons reducing protons generate hydrogen gas (**Fig. 1**) [9,10,14–16].

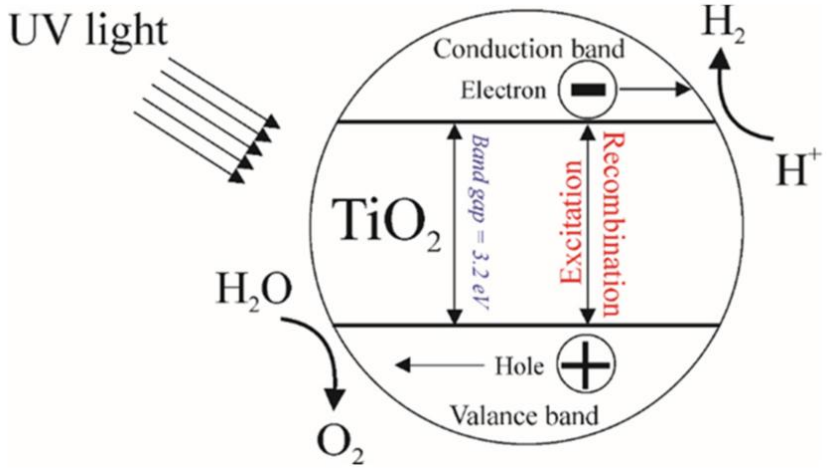


**Fig. 1.** Mechanism of water splitting in the production of hydrogen on a $TiO_2$ photocatalyst [17].

This method is desirable in the production of „green“ hydrogen gas, which is a carbon-neutral fuel, utilizing renewable solar energy and a stable semiconductor catalyst, without compromising on efficiency or increasing costs [15]. These versatile properties have also pushed the development of multifunctional surfaces, integrating self-cleaning, superhydrophobic and antimicrobial capabilities into coatings and textiles [18–20].

### 1.1.2. Structure and phases of titanium dioxide

The properties of $TiO_2$, as well as its efficacy, depends on the morphological and structural characteristics, which are intrinsically tied to the route of synthesis used and the parameters under which fabrication or post-fabrication processing is being done, most notably annealing temperature [16,21,22]. While maintaining the same chemical formula, structurally, the oxide exists in three distinct crystalline phases: rutile, anatase and brookite [16,23]. They differ from one another by the arrangement of $TiO_6$ octahedra within the crystal lattice (**Fig. 2**). Each of the $Ti^{+4}$ ions are surrounded by six $O^{2-}$ ions, the shape of the octahedron differing for separate $TiO_2$ phases [24].

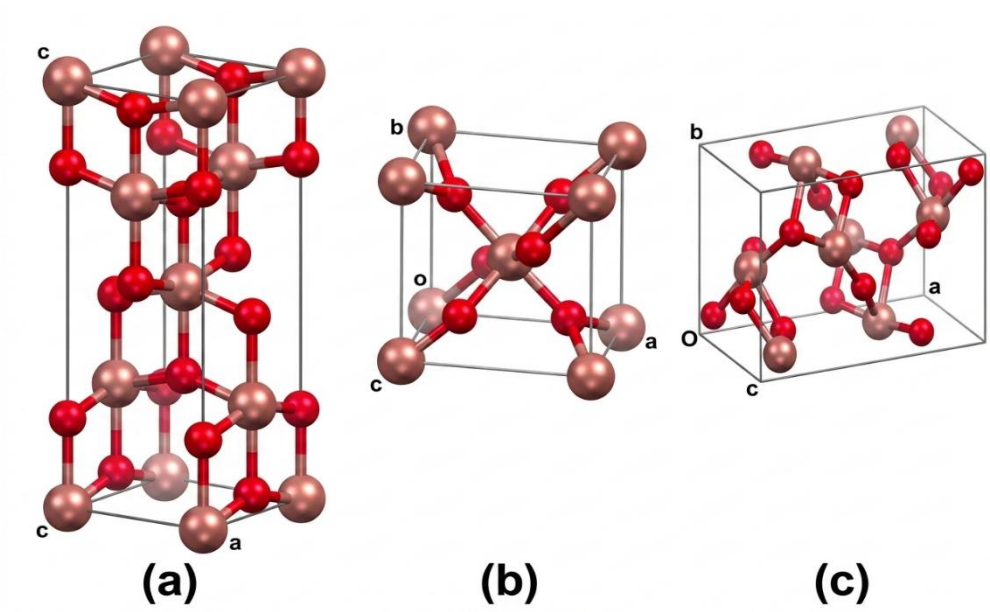


**Fig. 2.** Crystal structures of $TiO_2$: a) anatase, b) rutile and c) brookite. Pink color representing $Ti^{4+}$ ions and red color representing $O^{2-}$ ions. Modified from [25].

Anatase is characterized by a tetragonal structure. It is considered the most photoactive phase. This superior property is attributed to its lower electron-hole recombination rates and a higher density of surface active sites, which facilitate stronger interaction with target molecules and bacterial cells [22]. On the atomic scale, the distances between Ti–Ti atoms are greater in anatase, than in rutile, while distances between Ti–O are shorter. This difference determines the form and density between the phases of $TiO_2$ [26]. Additionally, in anatase phase, each $TiO_2$ octahedron chares four edges with neighboring octahedra, making the mobility of charge carriers more favorable structurally [24,27,28]. Rutile exhibits the same tetragonal structure as anatase, despite the difference in atomic distances of Ti–O, however, it is more responsive to near-ultraviolet wavelengths due to a narrower bandgap (~3.0 eV). In comparison to anatase, rutile shows less photocatalytic activity due to faster charge carrier recombination, however, it remains the most thermodynamically stable phase [8,16,26,29]. Brookite, the most complex and rarest of the polymorphs, crystallizes in an orthorhombic configuration. It remains infrequently utilized in industrial applications due to difficulty in manufacturing and maintaining its phase purity during fabrication, despite having high photocatalytic activity [21].

Point defects, such as oxygen vacancies, in the crystal lattice can influence the structural changes of $TiO_2$, participating in the reorganization of $TiO_6$ octahedra (**Fig. 3**) [27]. Atomic rearrangements and changes in structure are more frequent with the increasing density of vacancies, leading to phase changes being delayed when annealing is performed in low-oxygen environments [30].

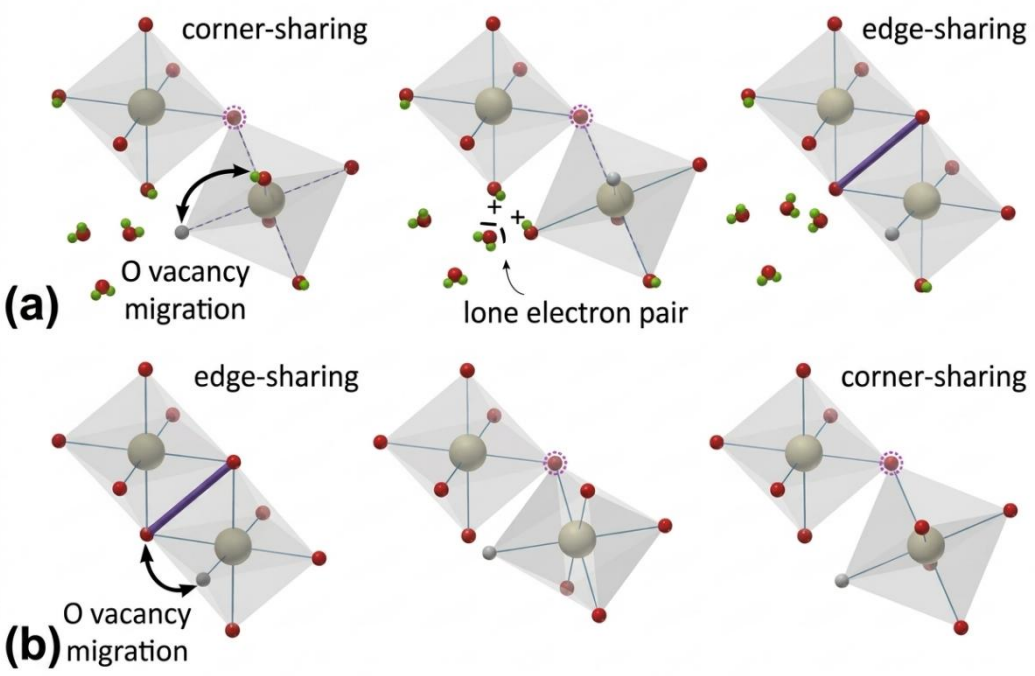


**Fig. 3.** Reorganization of $TiO_6$ octahedral connectivity. a) Edge-sharing connection formation from $TiO_6$ octahedra sharing a corner and b) Corner-sharing $TiO_6$ octahedra formation from edge-sharing octahedra due to oxygen vacancy migration. Modified from [27].

The electronic properties of the material vary greatly in accordance with its changing structural variations. The point defects in $TiO_2$, where the crystal structure is defected and missing atoms, contribute to the electrical properties. The missing oxygen atoms in the lattice result in the increasing electrical conductivity, wider range for light absorption and more active sites for the absorption of $CO_2$ [27,31].

### 1.1.3. Mechanism of photocatalysis

The antibacterial effects of $TiO_2$, regardless of the structure, are linked with the photocatalytic performance of the semiconductor. The mechanism of photocatalysis is based on electrons escaping from the valence band of the semiconductor to the conduction band, leaving behind a positively charged hole. The pairing of the electron and hole, also known as an exciton, facilitate oxidation and reduction reactions, that allows $TiO_2$ to split water molecules (**Fig. 4**) [31,32].

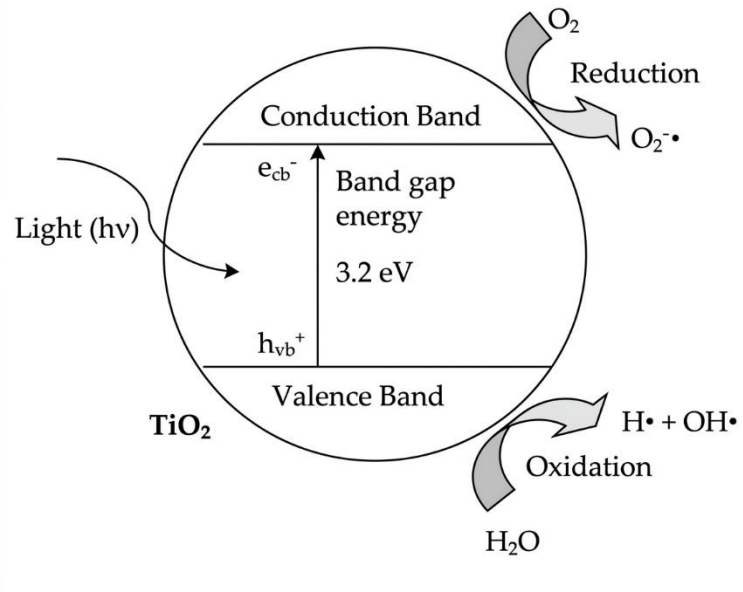


**Fig. 4.** Mechanism of photocatalysis under UV light in $TiO_2$. Modified from [33].

With sufficient energy coming from light, the photocatalytic mechanism produces various compounds from interactions with water and dissolved oxygen molecules through a set of sequential reactions [32,34,35]. They are the following:

$$TiO_2 + h\nu \rightarrow e^- + h^+ \quad (1)$$

$$H_2O \rightarrow O_2 + 4H^+ + 4e^- \quad (2)$$

$$h^+ + OH^- \rightarrow \cdot OH \quad (3)$$

$$e^- + O_2 \rightarrow O_2^- \cdot \quad (4)$$

$$2HO_2 \cdot \rightarrow O_2 + H_2O_2 \quad (5)$$

The generated ROS, such as hydrogen peroxide ($H_2O_2$), hydroxyl radicals (·OH), superoxide anions ($\cdot O_2^-$) and singlet oxygen ($^1O_2$) cause intracellular damage in microorganism cells, tumor cells, and the degradation of pollutants by oxidative processes [32,36,37].

### 1.1.4. Bandgap engineering

As previously mentioned, $TiO_2$ is photocatalytic when irradiated with UV light. However, the wide bandgap and rapid recombination of exciton pairs is not favorable for certain applications. One of the options for increased bandgap efficiency is using a combination of $TiO_2$ phases. Mixed-phase photocatalysts, for instance anatase-rutile heterojunction, have comparatively better performance. The increase in effectiveness is due to the „synergistic effect“ of both phases, however, the percentage of each phase in the mixed phase $TiO_2$ determines the optoelectronic and chemical properties which are exhibited [30,32,37,38]. Mixed-phase $TiO_2$ can exhibit better photocatalytic performance as the different conduction and valence band alignment allows for charge transfers at the interface [39,40]. The effective bandgap energy of anatase-rutile mixed-phase compounds is less than that of pure phase $TiO_2$, however, the ratio of the phases influences this phenomenon greatly, making the

optical bandgap tunable to a certain extent [39,41]. Due to its lower conduction band energy, the introduction of rutile can also reduce the fast electron-hole pair combination rate of anatase. Photoexcited electrons, after irradiation with UV light, transfer from anatase to rutile due to different alignments of conduction and valence bands, allowing charge transfers at the interface [39,40]. This option, however, requires high precision in fabrication and exact phase ratio distribution to achieve the desired photocatalytic effect [41].

The bandgap energy of $TiO_2$ can also be modified through the use of additional materials, such as metals, nitrogen and carbon structures. The addition of these compounds narrows the bandgap and allows for the $TiO_2$ to be functional under visible light, increasing efficiency (**Fig. 5**) [11,42–44].

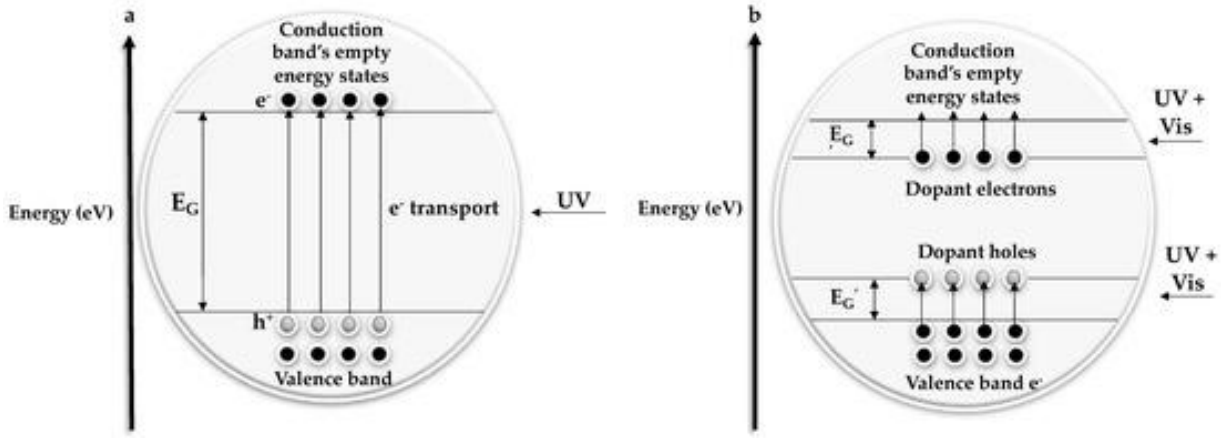


**Fig. 5.** Dopant effect on the electronic band structure of $TiO_2$, where $E_G$ is energy gap [45].

Introduction of dopants adds new energy levels between the conduction and valence bands of $TiO_2$, additional defect sites and decreases the recombination of electron-hole pairs while increasing charge carrier lifetime [46,47]. Dopants, like noble metals, also introduce Schottky barrier formation, electron trapping and localized surface plasmon resonance effects, which increase photocatalytic effectiveness under visible light [44,48]. The fabrication of the dopants and the consequent influence it has on the effectiveness in application must be analyzed to obtain the best desired result.

## 1.2. AgNP modification and fabrication

### 1.2.1. Mechanism of photocatalysis enhancements using AgNPs

The photocatalysis enhancing properties of metal nanoparticles are due to various phenomena they exhibit that bulk material does not. Noble metal particles, such as silver (Ag) and gold (Au), have the property of localized surface plasmon resonance (LSPR) and the formation of the Schottky barrier which influence the bandgap energy and charge carrier interactions with $TiO_2$ [49]. LSPR is a phenomenon that describes the collective oscillation of the electron cloud (**Fig. 6**) at the surface of the nanoparticle, specifically in the conduction band while interacting with an electric field or induced by photon energy [48,50,51]. There are several interactions that attribute to increased efficiency of $TiO_2$ photocatalysis using AgNPs, that are dependent on the light irradiation wavelength.

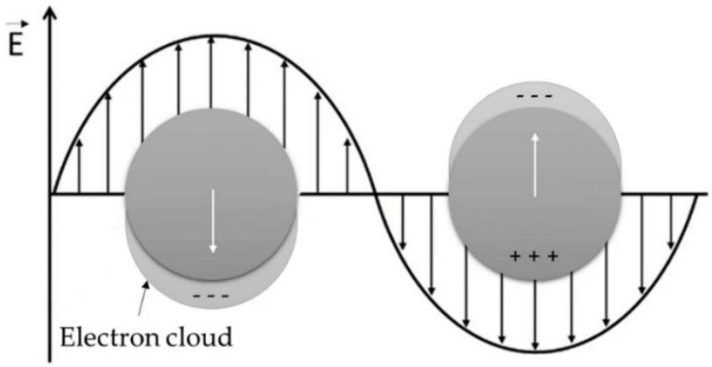


**Fig. 6.** Schematic interpretation of localized surface plasmon resonance phenomena in AgNPs. Modified from [50].

Under UV light irradiation, the photocatalytic effect of $TiO_2$ is activated and electron/hole pairs are generated. If the metal and the semiconductor come into contact, as they would if $TiO_2$ gets doped with AgNPs, due to equilibration, the electrons being to flow from the semiconductor to the metal. This, in turn, enables the formation of the Schottky barrier at the interjunction of the AgNP and $TiO_2$. The Schottky barrier formation allows the electrons to get trapped in the AgNPs. For this to occur, the Fermi level ($E_F$) must be higher for the semiconductor before the contact, while the work function of the metal ($\varphi_M$) is greater than the electron affinity ($E_x$) of the semiconductor (**Fig. 7**). This flow continues until equilibrium is reached [48,52,53]. This interaction allows for positive holes to be left on the surface of $TiO_2$ while AgNPs gather electrons and therefore inhibiting recombination, which allows more efficient ROS generation [53].

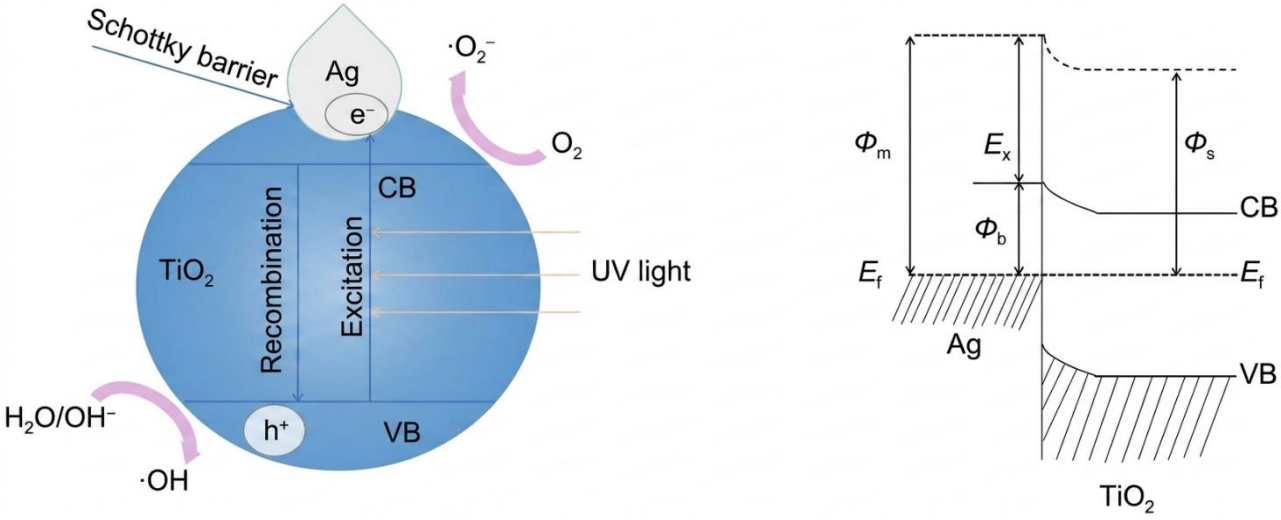


**Fig. 7.** Enhanced photocatalysis mechanism of $TiO_2$ and Ag due to formation of the Schottky barrier, where $\varphi_b$ is the Schottky barrier, $\varphi_m$ is work function of Ag, $\varphi_s$ is the work function of $TiO_2$, $E_x$ is the electron affinity, $E_f$ is the Fermi level, CB is conduction band and VB is valence band. Modified from [53].

Under visible light, the phenomena of LSPR occurs, in which the incident photons matching the frequency of the metal NPs cause the collective oscillation of free electrons in the metal conduction band. After the LSPR effect is induced, the electrons can move opposite, from the metal to the semiconductor instead, increasing the amount of charge carriers in the $TiO_2$ to produce ROS. Additionally, the interaction with the electromagnetic fields, that occur

around the nanoparticles, can also increase the amount of electron-hole pairs generated in the semiconductor [48].

The plasmonic resonance can lose energy by transferring it to individual electrons within AgNPs. These electrons, when contact between semiconductor and metal is maintained, will transfer to the conduction band of $TiO_2$ and diffuse or recombine with the holes there, as they lose energy and are unable to go back to the metal nanoparticle. The process of the hot electron injection is possible in visible light wavelengths (~400 nm), that pure $TiO_2$ is not responsive to, therefore increasing the absorption [31,48,50]. LSPR bands for AgNPs occur in the blue light range of the visible spectrum, thereby enhancing the range of absorption of light by AgNP+$TiO_2$ systems. The position of the LSPR peak can shift with the differing particle size to a bigger wavelength, a process called redshifting [50].

The wavelengths of the plasmon resonance differ based on the structural differences of AgNPs, along with their distribution and the concentration on the substrate, which can be modified through fabrication [50]. In order to utilize AgNPs for antibacterial applications, it is important to determine the right method that allows increased LSPR effect, while not diminishing the photocatalytic activity of $TiO_2$.

### 1.2.2. Fabrication of AgNPs

There are various methods of producing AgNPs on thin films, such as photodeposition, sol-gel spin coating, and physical sputtering methods [52,54,55]. In order to obtain the best qualities for antibacterial applications, magnetron sputtering is frequently utilized for fabrication, as it achieves high adhesion, uniformity and allows for precise control over distribution of films [56]. The ability to choose each fabrication parameter for magnetron sputtering and post-deposition treatments is highly advantageous for faster production rates, uniform coverage for larger areas while achieving films with specific qualities in mind [57].

Magnetron sputtering allows for the fabrication of $TiO_2$ films and the deposition of Ag onto $TiO_2$ films without disruptions. Switching of sputtering targets inside the chamber, without introducing outside air and particles, keeps the films contaminant-free and ensures less variability in production [57,58]. Using high purity targets in a vacuum chamber with constant rate and ratio of argon and oxygen gas, ensures controlled oxygen interactions with $TiO_2$, while avoiding unnecessary contamination using inert Ar gas. For AgNP fabrication, oxygen is excluded to avoid oxidation of silver [58,59]. To ensure that the surface of the target is without contaminants and the resulting films are without defects caused by intrusion of foreign atoms, the target is pre-sputtered [57]. Working pressure in the deposition chamber has an effect of the thickness of the deposited films [60]. With less working pressure, the thickness of the films increases due to the decreasing mean free path and less surface mobility of the sputtered atoms [61].

AgNPs are formed when the sputtered layer of Ag is annealed by keeping the films under high temperatures for a specific amount of time. The process is called solid-state dewetting. The method is explained by the formation of islands and finger-like or wire-like structures from the initial flat layer of deposited metal, which form into nanoparticles on the surface of the film [52,62]. Initial layer thickness of the deposited Ag film influences the size, shape and distribution of the formed AgNPs, with a thicker layer resulting in larger nanoparticle size

and irregular shape [62]. Different temperatures have an effect on the nanoparticle size, shape and surface characteristics as well. After annealing, the mobility of atoms increases, which leads to the agglomeration of small grains into larger ones, therefore, increasing surface roughness [57]. Further increasing the annealing temperature yields the larger, irregular nanoparticles to split into smaller, more spherical ones [62].

The large surface area of $TiO_2$ obtained with magnetron sputtering allows for increased photogeneration of electron-hole pairs, however, the addition of AgNPs in a large quantity can decrease photocatalytic abilities. Large concentrations of AgNPs deposited on the surface can cover the $TiO_2$ and prevent the absorption of photons, therefore, decreasing the generation of ROS and antibacterial effectiveness [63]. It is important to determine the right concentration of AgNPs with the initial layer thickness to achieve the highest possible antibacterial effect without diminishing returns and unnecessary use of noble metals. The determination of the antibacterial effect efficiency relies on our understanding of the mechanisms behind which the effect occurs.

## 1.3. Antibacterial mechanism

### 1.3.1. ROS interactions with bacteria

The antibacterial efficacy of $TiO_2$ thin films doped with AgNPs relies on several mechanisms. Primarily, the bactericidal process of the generation of ROS and their interactions with bacteria structures, however, supplemental silver ion cytotoxicity has shown to contribute to the process as well. Generated highly reactive species, such as hydroxyl radicals (·OH), superoxide anions ($\cdot O_2^-$) and hydrogen peroxide ($H_2O_2$) interact with the organic components of the bacterial cell wall, membranes and intracellular components, causing damage and decreasing vitality [41]. The mechanism differs based on the structural characteristics of the bacteria (**Fig. 8**). Gram-positive bacteria cell wall consists of a thick outside peptidoglycan layer that contains the intracellular components within the cell. Comparatively, Gram-negative bacteria have a much thinner peptidoglycan layer, however, they also possess an additional outer membrane of lipids, which protects the cell and provides better structural integrity and rigidity while maintaining ion balance [64].

These structural differences play a role in the reactions and bactericidal efficiency of AgNP+$TiO_2$ systems, as it determines the susceptibility to $Ag^+$ ions and reactive species by the bacteria and the inherent sensitivity to antimicrobial activity [64,65].

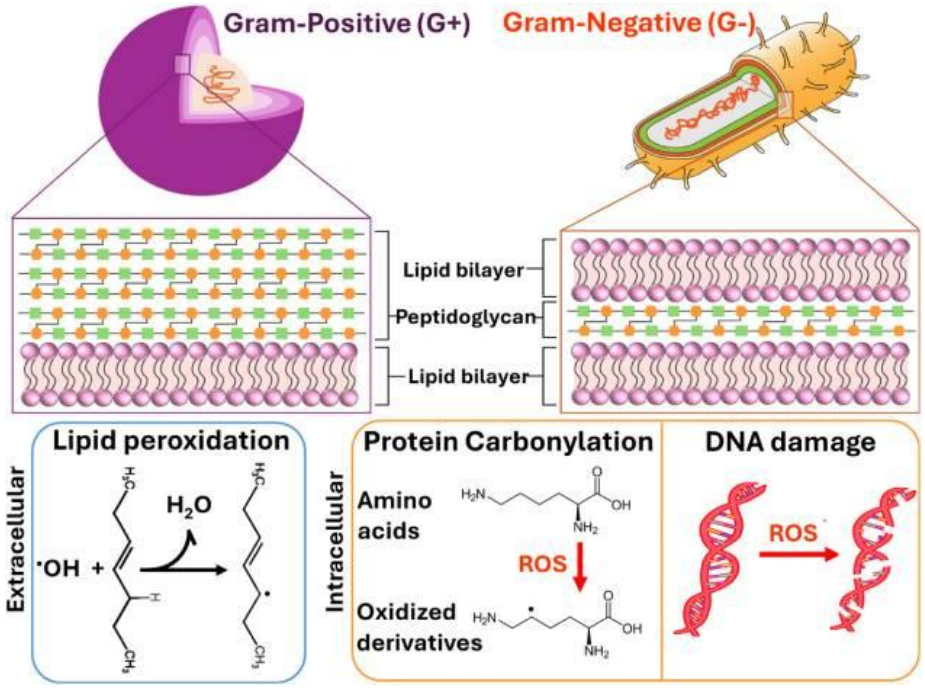


**Fig. 8.** Schematic of ROS-mediated damage to Gram-positive and Gram-negative bacterial cells [64].

As previously mentioned, there are several mechanisms that determine the antibacterial efficacy of AgNP+$TiO_2$ systems. The main mechanism, responsible for bacterial cell death is ROS-mediated oxidation of organic structures. These highly reactive species, produced by electron/hole pair interactions with oxygen and water molecules at the surface of the film, induce high oxidative stress onto the cells [36]. For Gram-positive cells, ROS causes the destabilization of peptides and polysaccharides of the peptidoglycan layer, as the layer is more chemically penetrable than the lipid bilayer [64]. The lack of additional lipid bilayer, that Gram-negative cells possess, makes Gram-positive bacteria more susceptible to ROS damage [66]. This difference allows for the oxidation of teichoic acids in the cell wall, making it weaker and increasing permeability. The additional outside layer of Gram-negative bacteria provides additional protection against ROS, however, ROS induced lipid peroxidation of the lipopolysaccharide layer and the phospholipid bilayer is still possible under higher concentrations of ROS, due to overwhelming oxidative stress [38,64,67]. Due to the damage of the cell wall, the internal components become exposed to ROS effects as well, resulting in DNA damage, protein carbonylation and lipid peroxidation. The damage to the cell walls also result in vital components leaking from the cell and reducing viability [36,38]. Bacteria may also reduce the effect of ROS by the production of antioxidants within the cell, however, they are only effective for short-term oxidative conditions, resulting in inevitable damage to cell structures and components [64].

### 1.3.2. Synergistic bactericidal effect of AgNPs

AgNPs provide a synergistic bacterial killing mechanism in AgNP+$TiO_2$ systems. $Ag^+$ ions can be dissociated from nanoparticles and interact with bacteria, causing additional damage to occur in the cells. Soluble ionic silver is produced when AgNPs interact with oxygen molecules and hydrogen in the environment. The oxidized surface of the AgNPs partially dissolves and becomes reactive, releasing $Ag^+$ ions into the environment until an equilibrium is reached [68]. These ions aid in the bactericidal effects due to their cytotoxic properties.

Interactions of $Ag^+$ ions with the bacterial cells can disrupt metabolic pathways. In smaller concentrations (μmol) $Ag^+$ ions disrupt molecular signaling, ATP synthesis and respiratory chains, while larger concentrations (mmol) can cause structural damages to the cell and DNA [66].

AgNPs are also known to interact with bacteria directly, without the release of $Ag^+$ ions, by binding to enzymes, membrane surfaces, and their functional groups, which interfere with the natural mechanisms of bacteria. AgNPs can adhere to the bacterial cell membrane influencing permeability and interfering with respiratory and other molecular transfer pathways [67,69,70]. AgNPs, depending on their particle size, can also directly enter the cell through the membrane, causing damage to the DNA and ribosomal biogenesis, however, even larger nanoparticles induce oxidative stress in the cell and lead to cell lysis or induction of apoptotic mechanisms [70,71]. Smaller AgNPs can also inhibit the creation of biofilms, which protect the bacterial cells from environmental stressors. $Ag^+$ ions and AgNPs smaller than 50 nm can disrupt the production of exopolysaccharides, allowing them to pass through to the cell wall and cause damage to vital structures [71].

Due to different interaction mechanisms of AgNPs and $TiO_2$ with the bacterial cells, it is important to characterize the microorganisms beforehand as their growth dynamics, biological mechanisms and structure can influence the antibacterial effect and bactericidal efficacy. Various computational methods allow us to model such attributes and their interactions with thin films, allowing us to understand the possible mechanisms before exploring real-life interactions.

### 1.4. XDLVO theory

The antibacterial mechanism of AgNPs on $TiO_2$ films relies on the surface interactions with bacteria. Bacteria have to be in contact with the film to enable the ROS to damage the cell surface, therefore, one of the most important aspects to consider is adhesion. Mathematical models are able to describe the surface adhesion interactions between microorganisms and thin films that influence the antibacterial effectiveness [72].

One of the theories used for modelling interactions is called the Derjaguin-Landau-Verwey-Overbeek (DLVO) theory. It is used to describe the forces between two surfaces, such as electrostatic (EL) or Lifshitz-van der Waals (LW) interactions, however, it assumes that the surfaces are inert chemically, which is not the case for anatase $TiO_2$. It is ideal for describing colloidal solutions, however, with bacterial suspensions, the introduction of extracellular polymers and chemical bonds complicates the theory and requires additional variables [72,73]. The DLVO theory can be expanded to include the Lewis acid-base (AB) interactions that would help explain non-covalent forces that occur between biofilm of bacteria and the surfaces on which they reside. The sum of the LW, EL and AB forces allows us to determine conditions under which adhesion is the strongest or weakest [74]. The total surface interaction energy between the bacteria and the substrate can be described as such:

$$W_{Tot} = W_{LW} + W_{EL} + W_{AB} \quad (6)$$

where, $W_{Tot}$ is the total energy of interactions, $W_{LW}$ is the Lifshitz-van der Waals interaction energy, $W_{EL}$ is electrostatic interaction energy and $W_{AB}$ is the Lewis acid-base interaction energy.

Repulsion forces between bacteria and the film can increase distance, making the ROS unable to reach the cells, however, increased adhesion can irreversibly attach the bacteria to the surface [72]. Primarily, closer to the surface of the film, van der Waals interactions are dominant, allowing the initial attraction to the surface. Further away from the film, repulsive Coulomb interactions begin to repel bacteria from the surface, due to the electrical double layer formation. While in theory, these forces ensure that bacteria do not adhere to the surface, counter measures of the bacteria, such as eDNA extrusion of the electrical barrier and the excretion of biofilm forming, glue like compounds, allows for increased adhesion [75]. For this reason, it is important to consider expanding the XDLVO theory to include these biological changes, as they directly influence the chemical bonds between the substrate and the cell. The suspension in which the bacteria reside, has various ions and a specific pH level to maintain cell viability during testing and control osmotic shock along, however, this influences the charge of the film and the cell wall, increasing interaction complexity [75].

The surface thermodynamic theories help us better understand the formation and qualities of biofilms that would be difficult to predict experimentally. Determination of parameters that are used for interaction models stems from investigations of specific microorganisms of interest. Their physical attributes and biological properties allow us to be precise and accurate with simulations. It is important to understand the structure and biology of a bacteria to explain how it influences the adherence kinetics to thin films.

## 1.5. *Bacillus subtilis* as a biological model

### 1.5.1. Biology of *B. subtilis*

In order to evaluate the antibacterial efficiency of AgNPs and $TiO_2$, various microorganisms have been used in research. Traditionally, Gram-negative bacterial strains, such as *Escherichia coli* and *Pseudomonas aeruginosa,* alongside Gram-positive *Staphylococcus aureus* serve as primary model organisms, due to their prevalence in clinical infections and ease of cultivation[76–79]. While antibacterial efficacy testing with pathogenic bacteria closely replicates conditions under which the films would be utilized, there are several biosafety concerns. Gram-positive *Bacillus subtilis*, having the status of Generally Regarded as Safe (GRAS), offers a comprehensive and safer alternative for antibacterial testing [80]. *B. subtilis*, a non-pathogenic aerobic bacteria commonly found in soil, is widely used in industrial applications, including fermentation of foods, manufacturing of supplements and animal feeds [81,82]. Not unlike other model organisms, such as *E. coli*, *B. subtilis* has a rapid growth rate in nutrient rich environments and can double in concentration within 30 minutes. High nutrient availability allows the bacteria to maximize the synthesis of ribosomes, prioritizing the allocation of proteome resources, while the synthesis of proteins unnecessary for rapid growth decrease [83]. The beginning of the growth cell cycle is linked with the elongation of the cell sidewalls and by the forming of the septum at the midcell of the bacteria. These mechanisms are controlled by actin homologues present in the genome of Gram-positive bacteria. The thick peptidoglycan walls of the Gram-positive bacteria allows the cells to remain a consistent diameter [84].

### 1.5.2. Sporulation

Due to nutrient limitations or unfavorable growth conditions, *B. subtilis* can form spores that protect it from harsh environmental factors. The effect of sporulation is activated by Spo0A regulator, inducing population heterogeneity and sibling cell cannibalism [85]. Sporulation happens in several well documented stages (**Fig. 9**).

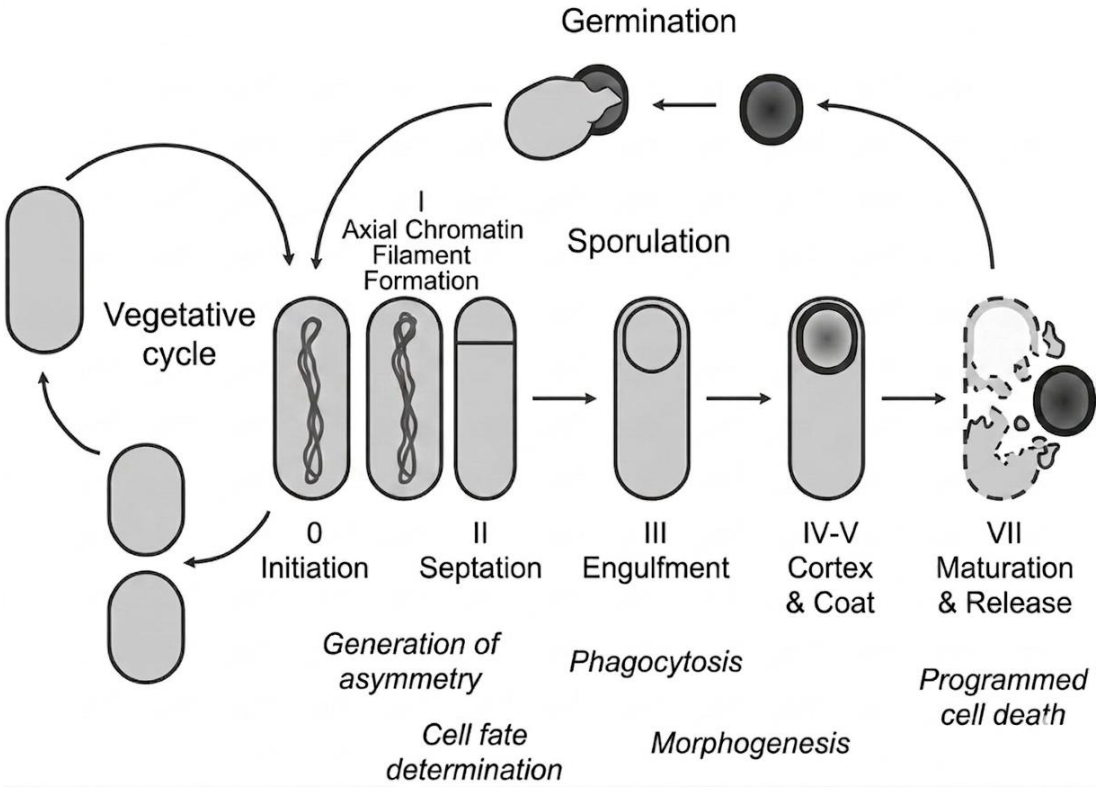


**Fig. 9.** Schematic diagram of *B. subtilis* sporulation stages. Modified from [86].

During the initial stages, the bacteria are in a vegetative state, until Spo0A is activated. Sporulation starts with the axial chromatic filament formation in the cell, followed by septation. After the spore septum forms, the spore membrane develops, allowing the forespore to be released inside of the main mother cell. Stages IV and V encompass the formation of the cortex and spore coat, which protects the internal chromatic structures within. Lastly, the spore matures and is released from the mother cell, while the remainder of the cell autolyzes [85,87]. Dormant spore states are reversable when conditions become favorable again. Under environmental stimulus, such as amino acid introduction or high pressure, and adequate nutrition the spores germinate back into vegetative cells [82]. Nutrient availability is crucial in the formation of spores and colonies. Compounds such as organic nitrogen sources, complex carbon sources, such as starch, and inorganic salts increase spore formation due to difficult absorption and induction of starvation of the cells [82].

Since *B. subtilis* is non-pathogenic, it allows for the testing of sporulation, spore inactivation and other mechanisms of related species, like *B. anthracis* or *C. botulinum*, without posing serious health risks [88]. The spores of *B. subtilis*, due to their non-pathogenic nature are ideal for testing food processing and water disinfection systems [88,89]. The incredible resistance of *B. subtilis* spores in harsh environments make it ideal for testing the antibacterial efficacy of thin films.

While currently, much of the research is focused on vegetative, simple structured cells, real-life applications require rigorous testing with more dormant states of bacteria. Another component that needs to be taken into consideration is the formation of biofilms, which are prevalent with bacteria such as *B. subtilis*.

### 1.5.3. Biofilm formation

The ability of *B. Subtilis* bacteria to form biofilms is a major point of interest. The strain has been widely studied for this reason, due to its ease of cultivation and ability to start producing biofilms under specific controlled conditions [90]. Biofilm formation begins with surface interactions. The previously mentioned initial adhesion interactions with the films are reversable up until the distance between the bacteria and the surfaces decreases to less than 1.5 nm. This promotes the development of irreversible attachments that bond the bacteria to surfaces. After irreversible adhesion begins and the density of bacteria reaches a certain point, genes are expressed to begin forming biofilms. Signals in the cell respond to this strong adhesion, inhibiting movement of the cell and promoting the production of extracellular polymeric substances (EPS) [75]. While different compounds and environmental parameters influence the structure and production of the EPS, the main properties remain the same. These EPS compounds function as an adhesive and a protective shield for the bacteria. Within the biofilm, the bacteria cells or spores have a better chance of survivability, since EPS helps with nutrient retention, keeping hydration levels, gene transfer and protection of enzymes outside of the cell [91,92]. The EPS also provide protection from ROS. Interactions with ROS results in increasing EPS production and quenching of the toxic compounds, however, this also increases the adhesion to the substrate, providing a chance for more interactions [91].

Within the biofilm, there are different phenotypes of *B. subtilis* bacteria. The differentiated cells, such as mobile, sporulating and matrix-producing, contribute to the appearance and structure within the colonies and biofilm. Biofilms containing large amounts of matrix-producing and spore forming bacteria are often called „mature“ and exhibit stronger adhesion properties and resistance to environmental stressors [81].

Research shows a lack of experimental validation of methods that would include mixed bacteria phenotypes and the formed biofilms, as certain mechanisms are explored only with isolated vegetative state cells, spores, or specific extracellular compounds.

## 2. Methods and Materials

### 2.1. Film fabrication parameters

The films were fabricated using a magnetron (PVD-75 Kurt J. Lesker) to ensure uniform films. The initial $TiO_2$ films were deposited using 250 W DC sputtering onto microscope glass slides as the substrate under a high vacuum created by turbo-molecular pumps. The chamber was kept at a constant pressure of 5 mTorr under an $Ar/O_2$ atmosphere, where the flow was kept at a 20/80 ratio. The holder was rotated at 8 RPM and time of deposition was maintained until 200 nm thickness of $TiO_2$ was achieved at a growth rate of 1.6 nm/min. After the preparation of the films, the temperature was kept at 500 °C for 1 hour to anneal the $TiO_2$ and achieve the anatase phase.

For the AgNP formation, the prepared $TiO_2$ films were sputtered with a 99.9995% purity Ag target using RF magnetron sputtering at 50 W power. The chamber was kept under a 2.0 x $10^{-1}$ Pa vacuum with a pure argon atmosphere to avoid oxidation of Ag. The same rotation was kept at 8 RPM, deposition time was maintained until the films formed initial layer thicknesses of 5 nm, 7.5 nm and 10 nm. Post deposition the films were annealed at 400 °C for 1 hour in order to perform solid-state dewetting and form nanoparticles.

### 2.2. Morphological analysis

The prepared $TiO_2$ and AgNP+$TiO_2$ films were analyzed by taking micrographs using an optical NIKON Eclipse LV100D microscope (Nikon Metrology Inc. Brighton, MI, USA) using 50x magnification. For AgNP+$TiO_2$ samples, dark-field parameters were applied. Micrographs were taken after the films were fabricated, post washing procedures required to collect bacterial suspension and after the films were cleaned and dried, to determine longevity of the films.

After the experimental method was completed and the bacterial suspension was rinsed off using 1/500 LB nutrient broth (NB) (Biotecha, Lithuania), the films were left to dry on the work surface. Afterwards, methylene blue was applied and kept on the films for 1 minute to stain any remaining bacteria or spores, after which it was rinsed off with distilled water and left to dry completely. Micrographs were taken of the stained films.

### 2.3. Water contact angle

Water contact angle measurements were taken before the films were used for experimentation. The films were cleaned with high-pressure air; a water droplet was deposited on the surface of the films and pictures were taken from the side. The acquired pictures were analyzed using ImageJ software.

### 2.4. XDLVO modelling

XDLVO modelling of bacterial interactions with films was done using MatLab software. The environmental condition parameters used were room temperature (estimated to be 25 °C), which using the Boltzmann constant (1.38 x $10^{-23}$), allowed us to calculate the environmental thermal energy. The radius of *B. subtilis* bacteria was estimated to be roughly 520 nm, as was used in calculations by Pajerski *et al*. (2019) [93]. Since the model needed to reflect the

experimental setup, the ionic strength (I) was determined for 1/500 NB. Initial bacterial suspension concentration (6 x $10^5$ CFU/ml) was based on the requirements of ISO 27447:2019 standard for test methods for antibacterial activity of semiconducting photocatalytic materials. Irradiation parameters were also taken from the ISO 27447:2019 standard, the chosen intensity (0.25 mW/$cm^2$) was the maximum intensity before UV irradiation damage could occur [94].

Several models were ran based on the XDLVO theory to explain the survivability of *B. subtilis* bacteria under testing conditions and interaction potential between the films and the cells.

## 2.5. Experimental Setup

### 2.5.1. Cultivation of *B. Subtilis*

For the antibacterial effectiveness testing and preparation of materials, a modified version of the ISO 27447:2019 standard was used. Solid agar medium was prepared using LB agar (Biotecha, Lithuania) according to instructions, 18.5 g of agar medium powder was melted in 500 ml of distilled water in an Erlenmeyer flask under constant stirring. The mixture was kept at boiling point for 30 minutes after turning translucent to ensure homogeny and provide a low level of sterilization. The agar nutrient medium was cooled to 50 °C before being poured into Ø9 cm Petri dishes and set on a flat surface to cool. Once solidified, Petri plates were transferred into refrigerator kept at a constant 4 °C.

1/500 NB was prepared according to instructions. 2.5 g of LB broth (Biotecha, Lithuania) powder was dissolved in 100 ml of distilled water to achieve a 1/1 NB solution. For 1/500 NB broth, 1 ml of 1/1 NB was diluted with 499 ml of distilled water. When not in use, the 1/500 NB broth was labeled and stored at 4 °C, before inoculation it was brought up to room temperature to avoid cold shock of the bacteria.

Initial bacterial suspension was produced by inoculating a nutrient agar plate from cryo-bead *B. subtilis* inoculum stored at -18 °C. From the culture, 2-5 beads were added onto the plate and rolled around the surface of the agar using a sterile loop. The plate was incubated at 37 ± 0.1 °C for 24 hours in a water jacketed incubator (Forma Scientific 3154 Water Jacketed Incubator, ThermoFisher Scientific, USA), an additional Petri dish with distilled water was added to ensure high humidity level in the incubator. Colonies grown from initial inoculation were collected using a sterile loop, streaked onto a fresh medium and incubated again for 24 h in the same conditions. The resulting colonies from the secondary sub-culture were used to make the bacterial suspension needed for $OD_{600}$ calibration curve measurements and the experimental section. The bacterial suspension was made by inoculating ~30 ml of room temperature 1/500 NB solution with 5-6 colonies, afterwards, the suspension was mixed until no visible clumps of bacteria were present. $OD_{600}$ measurements were taken to determine approximate bacterial cell count.

### 2.5.2. Calibration curve

Before the bacterial suspension was used for experiments, the relationship between transmittance at 600 nm UV wavelength and bacterial cell count was established. A stock solution was made by inoculating 10 ml of 1/500 NB solution with 10-15 colonies.

Transmittance measurements were taken using a USB400 spectrometer (Ocean Optics Inc. Rochester, NY, USA) (**Fig. 10**). Separate attachment was used for cuvette insertion for liquid measurements.

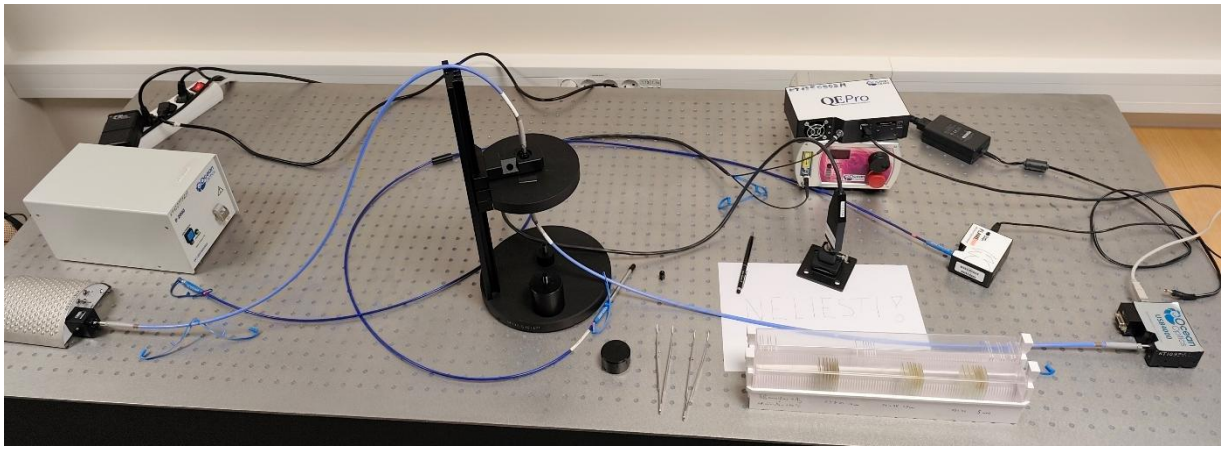


**Fig. 10.** Measurement setup for transmittance of samples using USB400 spectrometer.

Transmittance value at 600 nm ($\%T_{600}$) was recalculated to reflect optical density ($OD_{600}$) using this formula:

$$OD_{600} = 2 - log_{10}(\%T_{600}) \quad (7)$$

The bacterial suspension was diluted using additional 1/500 NB to reach an $OD_{600}$ measurement of 1. This stock solution was then used to perform dilutions with additional 4 suspensions (A-D) to achieve an $OD_{600}$ measurement of around 0.5, 0.25, 0.125 and 0.06. The stock suspension along with suspensions A-D were diluted further for plating to achieve viable cell counts by using 0.5 ml of the initial solutions in 4.5 ml of physiological saline. Stock solution ($OD_{600}$ = 1.001) was diluted to a factor for $10^{-6}$, A solution ($OD_{600}$ = 0.501) to a factor of $10^{-6}$, B solution $OD_{600}$ = 0.257) to a factor of $10^{-5}$, C solution ($OD_{600}$ = 0.120) to a factor of $10^{-4}$ and D solution ($OD_{600}$ = 0.065) to a factor of $10^{-4}$. For each of the solutions, 100 µl were plated onto agar medium and incubated for 24 hours. Colony count was performed for each of the plates and concentration was determined using formula (8):

$$CFU/ml = \frac{N_A/0{,}1}{DF} \quad (8)$$

where, NA is the average number of colonies on the agar medium and DF is the dilution factor.

A logCFU/ml as a function of $OD_{600}$ graph was drawn, from which the trendline formula was used to determine CFU/ml of bacterial suspensions used in experiments based on their transmittance measurements.

### 2.5.3. Irradiation setup

The experiment was set up based on the ISO 27447:2019 “Fine ceramics (advanced ceramics, advanced technical ceramics) – Test method for antibacterial activity of semiconducting photocatalytic materials“ standard [94]. Bacterial suspension was made using a fresh secondary sub-culture and concentration was evaluated following the same procedure described in section 2.5.2. The suspension was further diluted with 1/500 NB

solution to achieve an approximate concentration of 1 x $10^6$ CFU/ml. Bacterial suspension was used immediately after measurement to avoid concentration errors due to growth. A time zero ($T_0$) sample of 60 µl (100 µl for full plates) of prepared bacterial suspension was plated onto a Petri dish right before the test, to ensure the bacterial suspension used for the experiment was viable before being deposited onto the thin films.

Films were setup based on the ISO 27447:2019 standard (**Fig. 11**) [94]. A clean Petri dish was lined with paper towel and dampened with distilled water, cuvette lids were placed in the dish to raise the film off of the paper towel to avoid leaking of bacterial suspension or contamination. Glass slide was positioned in the center as evenly as possible to avoid leaks off the slide. 60 µl of the prepared bacterial suspension was placed at the center of the film and covered with a sterile square of LDPE plastic to ensure equal distribution of bacteria across the film. The lid of the Petri dish was placed on top to prevent drying.

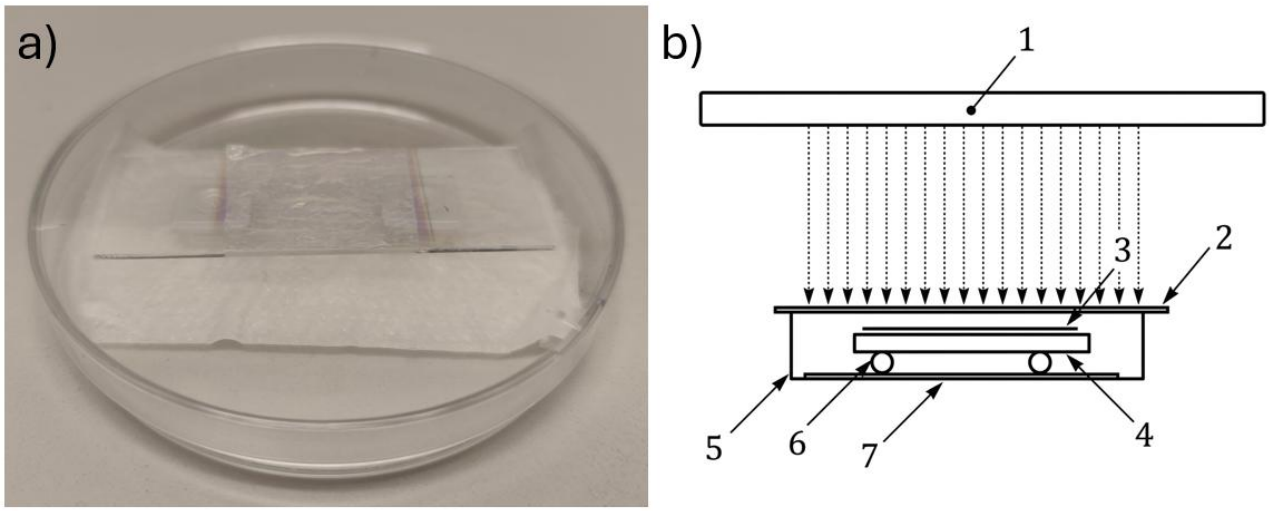


**Fig. 11.** Experimental setup (a) for antibacterial effectiveness testing based on modified ISO 27447:2019 standard (b) [94]. Labels indicate light source (1), Petri dish lid (2), LDPE cover film (3), Glass slide with film sample (4), Petri dish (5), cuvette lid stilts (6) and damp paper towel (7).

Experiment was carried out with 10 samples each time. Clean glass slides were used as control, while the films tested were pure $TiO_2$, AgNP+$TiO_2$ films where the initial thickness was 5 nm, 7.5 nm and 10 nm. Half of the samples were irradiated with a UV lamp that was kept at a 30 cm distance from the surface of the films, while the other half was wrapped in foil to avoid light irradiation, but kept on the same workspace to avoid environmental variables.

All samples were irradiated for 1 hour, after which the cover film was peeled off and submerged into 5 ml of washing liquid. The washing liquid was then pipetted onto the glass slide to remove any leftover bacterial suspension. 60 µl of the washing liquid was collected and plated onto fresh Petri plates. All samples were incubated for 24-48 hours before visually performing a viability check.

## 3. Results and Discussion

### 3.1. Physical properties of films

Water contact angle measurements were done with four different types of thin films: pure $TiO_2$ and three AgNP+$TiO_2$ films with varying initial layer thicknesses of 5 nm, 7.5 nm, and 10 nm respectively.

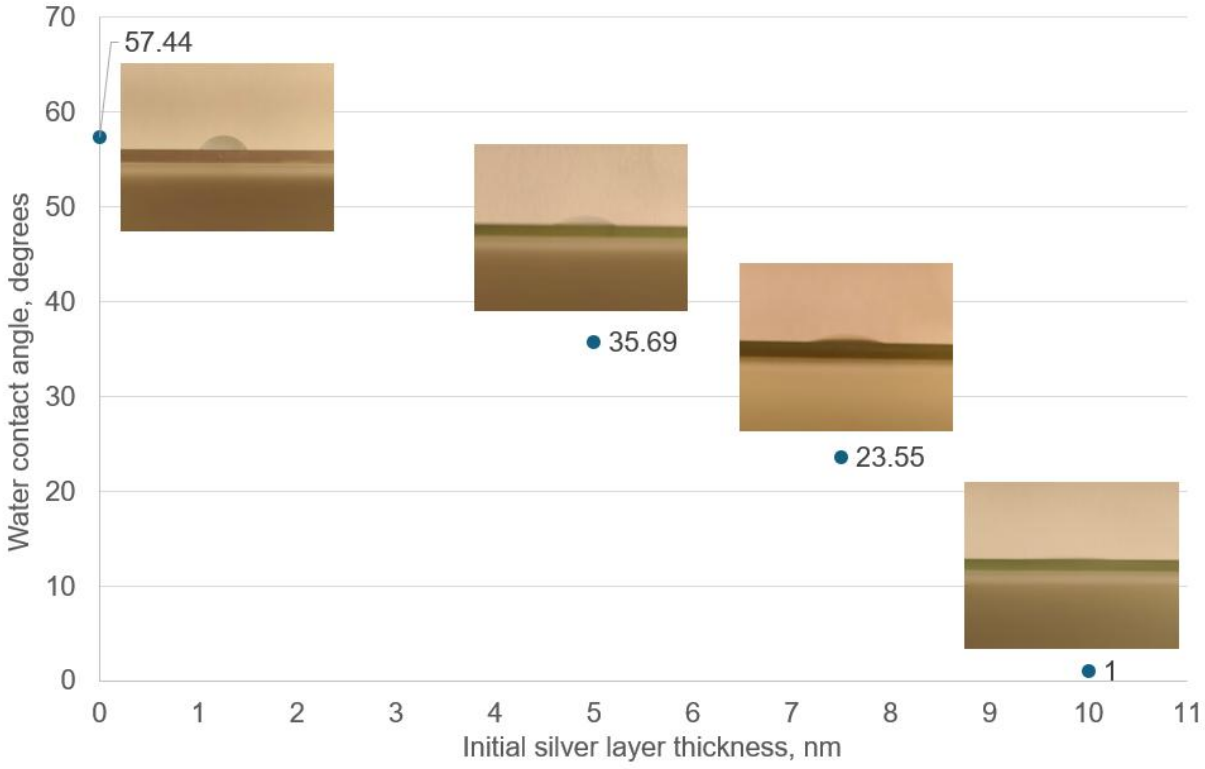


**Fig. 12.** Water contact angle dependence on initial silver layer thickness on thin films.

Based on the results, shown in **Figure 12**, there is an obvious dependence between surface wettability and AgNP concentration on thin films. With increasing AgNP content, the contact angle diminishes, in comparison to $TiO_2$, which was used as the baseline. The contact angle shifts from 57.44 degrees ($TiO_2$) to approximately 1 degree (10 nm initial Ag layer thickness) under visible light irradiation. This indicates superhydrophilic properties of $TiO_2$ films doped with AgNPs, which has been reported before in literature by Razak et al. (2020) and Nath et al. (2022) [95,96]. The increased wettability is a factor in antibacterial effectiveness of the films. Increased wettability allows for increased production of ROS due to higher surface spread of water, as well as more uniform spread of bacteria across the film, which allows for higher interaction rates with the generated ROS [95]. While superhydrophilicity has high hydrogen bonding effect, enabling it to form a hydrated layer and making it difficult for bacteria to adhere to the surface, the production of ESP in *B. subtilis* can counteract these measures [91].

### 3.2. Biological baseline

The relationship between absorbance and viable cell count was established to standardize the initial concentration of the bacterial suspension (**Fig. 13**)

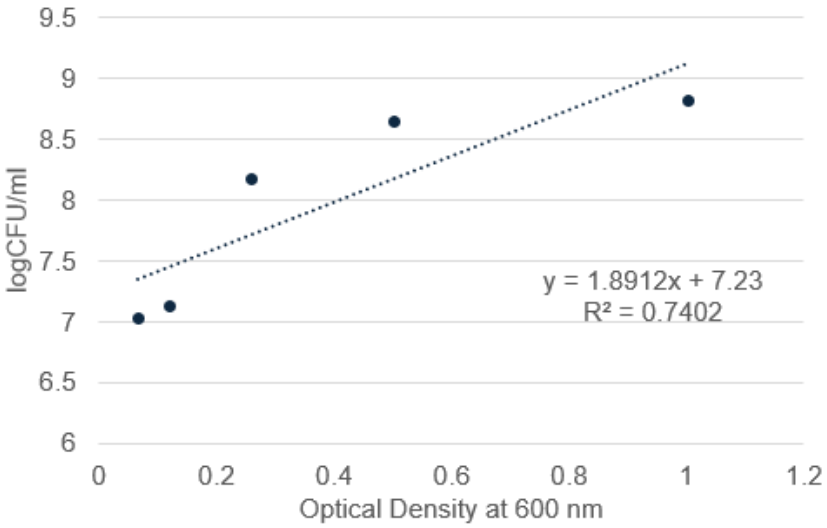


**Fig. 13.** Relationship between optical density ($OD_{600}$) and bacterial concentration of *B. subtilis* in 1/500 NB suspension (log CFU/ml).

**Figure 13** illustrates the calibration curve correlating the optical density ($OD_{600}$) of the bacterial suspension with the log-transformed colony-forming unit concentration.

The calibration curve exhibits a positive linear correlation, represented by the equation y = 1.8912x + 7.23. There is moderately strong correlation between concentration and optical density ($R^2$ = 0.7402), which is to be expected with inherent biological variability of colony forming and absorbance measurements.

The Petri plates used for CFU counting visually confirm the presence and viability of the bacteria (**Fig. 14**).

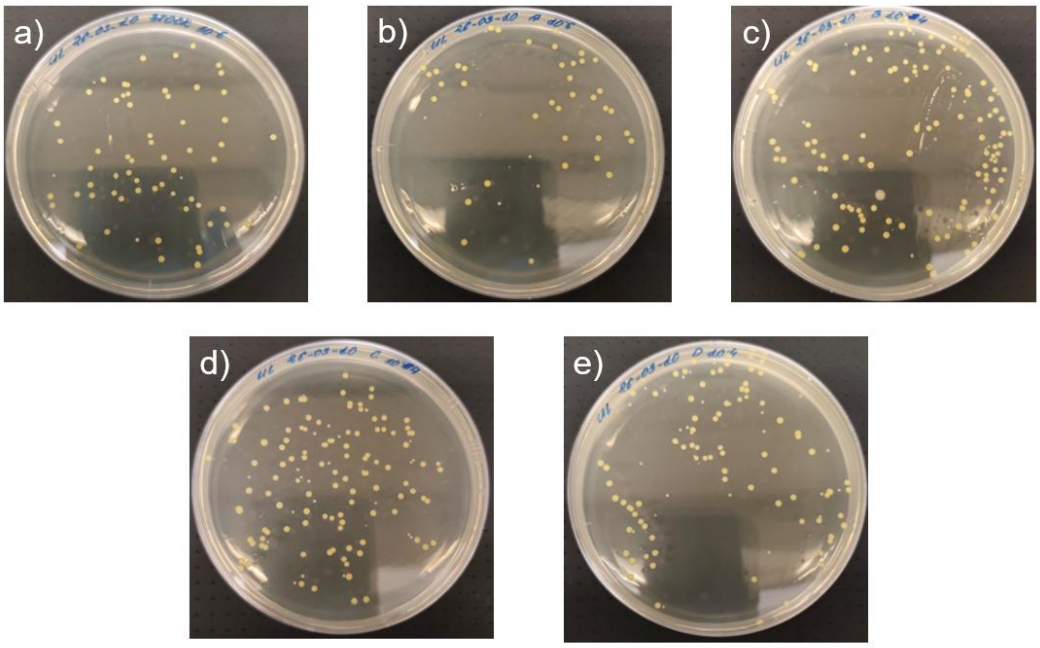


**Fig. 14.** Representative agar plates showing viable counts of *B. subtilis* colonies. Plated suspensions were prepared at dilution factors of a) $10^{-6}$, b) $10^{-6}$, c) $10^{-5}$, d) $10^{-4}$ and e) $10^{-4}$.

**Figure 14** represents the results of the spread plate method used to verify the concentration of the prepared bacterial suspension. Each Petri dish contains nutrient agar inoculated with a specific dilution of the culture to ensure it falls within the statistically valid countable range of 30-300 colonies per plate. The uniform spread of colonies confirms the homogeneity of the suspension and validates the bacterial suspension preparation and dilution protocols. The lack of contaminants present also confirms proper sterile technique. **Figure 13** and **figure 14** were used as a quantitative baseline for determining the initial CFU/ml of the bacterial concentration used in further experiments.

### 3.3. Experimental results

Experiments were carried out following the determined protocol detailed in section 2.5.3. Post-incubation visual check was performed to verify the methodology, however, there was a lack of positive control, which made it unable to compare results with accuracy. Initial experiments used 5 ml of physiological saline as a washing medium, as indicated by ISO 27447:2019 standard [94]. The $T_0$ growth plates (**Fig.15**) showed high viability in the initial bacterial suspension.

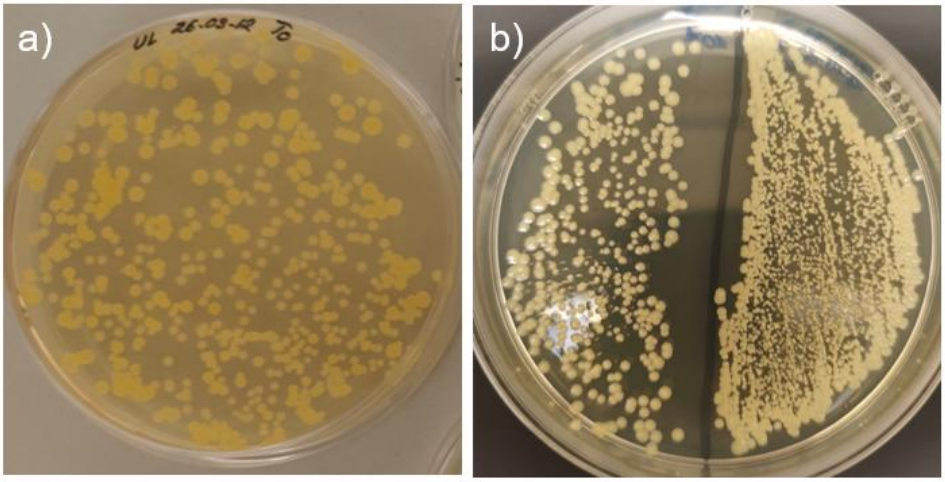


**Fig. 15.** Agar plates showing viable counts of *B. subtilis* colonies of initial bacterial suspension samples ($T_0$) of plated a) 100 µl of 1 x $10^6$ CFU/ml and b) 60 µl of 1 x $10^6$ (right) and 1 x $10^5$ CFU/ml (left) suspension.

Experiments were carried out using the bacterial suspension, however, this did not yield a positive control or showed any significant growth in any of other samples. The amount of washing medium was lowered to 1 ml to increase the viable colony count and reduce dilution. The same experiment was repeated with 5 ml and 1 ml of 1/500 NB solution as the washing medium, as it would ensure that the bacterial cells not only retain their osmotic balance, as with saline, but also be able to repair minor damages to the cell walls and remain stable, as they favor NB solutions [97]. All experiments yielded no positive control, therefore, further investigations were warranted.

### 3.4. UV lamp

Since initial experiments did not yield comparable results, other parameters of influence were analyzed. For the UV irradiation samples, the lamp used did not have specified parameters or clear range of wavelengths, therefore spectrometric analysis was warranted.

Based on the measured spectra, it was determined that the UV lamp range exhibits wavelengths from around 380 to 425 nm, peaking at around 400 nm. That is the typical range for UV LED lamps, commonly used for personal use, such as nail appliances. The wavelength range for these UV lamps encompasses the far range for UV-A (up to 400 nm, going into visible blue light (> 400 nm), which is not harmful enough to kill bacteria [98]. For photocatalytic applications this type of illumination would invoke the synergistic effect of both $TiO_2$ and AgNPs, however, there is no UV-C range wavelengths that would induce sporicidal or germicidal effects reported in literature [99,100]. Due to these results, we can eliminate the possibility that the UV lamp was bactericidal enough to cause all samples, including the control, to have no viable bacteria left.

### 3.5. Simulation

XDLVO modelling was done to see the effects that $TiO_2$ and AgNP+$TiO_2$ films have on the survivability of *B. subtilis* bacteria under UV and dark conditions (**Fig. 16**) as well as the XDLVO interaction potential that would explain the adherence of bacteria to films.

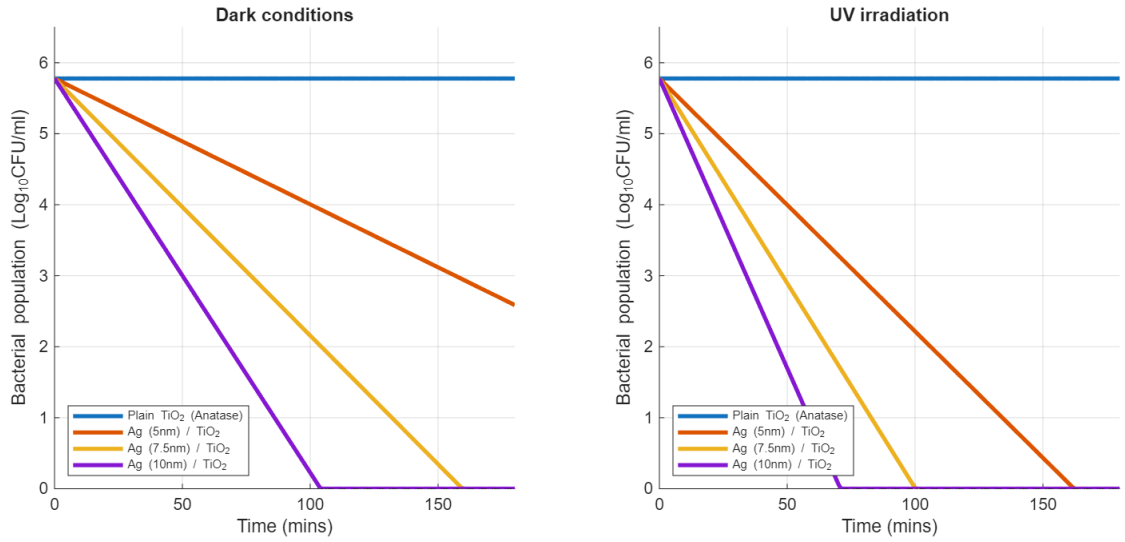


**Fig. 16.** XDLVO modelling graphs of bacterial survivability in based on time in contact with films under UV irradiation and dark conditions.

**Figure 16** shows the antibacterial effect of $TiO_2$ and AgNP+$TiO_2$ thin films under different illumination conditions. Anatase $TiO_2$ remains inert while samples with AgNPs show a concentration dependent reduction in the bacterial population. AgNP+$TiO_2$ sample activity can be attributed to the release of $Ag^+$ ions, which can interact with cell walls and cause death without light irradiation. Under UV irradiation, the killing rates of all AgNP doped samples accelerate. This can be attributed to the synergistic effect of photocatalysis driven ROS generation, narrowing of the bandgap and the remaining release of $Ag^+$ ions. Notably, the plain $TiO_2$ sample remains flat in both illumination conditions. The modelled electrostatic repulsion of bacteria and the surface of $TiO_2$ likely keeps the distance of interactions far enough away, that ROS does not reach the bacteria before decaying.

The interaction potential model was made to explain the interactions between the bacteria and the films that influenced the adhesion dynamics (**Fig. 17**).

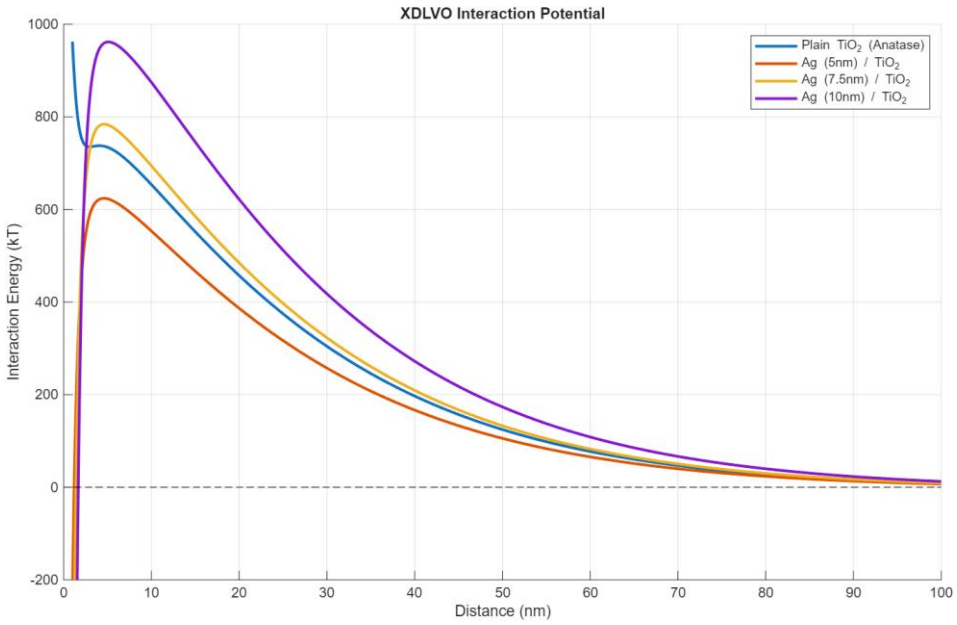


**Fig. 17.** XDLVO modelling of interaction potential between $TiO_2$ and AgNP+ $TiO_2$ thin films and *B. subtilis* bacteria based on distance.

**Figure 17** shows XDLVO interaction energy profiles that describe the adhesion potential between *B. subtilis* and various thin film surfaces. Each curve represents the total interaction energy ($V_{Tot}$), summed from van der Waals forces, electrostatic interactions and acid-base interactions, as a function of separation distance. The repulsive energy barrier predicts that bacteria will be hindered from reaching the primary minimum required to irreversibly adhere to surfaces and be affected by ROS. However, this model predicts ideal parameters of biological organisms, such as uniform spherical shape, lack of extracellular compounds or ions, as well as movement. As previously discussed, *B. subtilis* bacteria produces EPS, which are long-chain biopolymers extending far beyond the immediate radius of the cell. These EPS can adhere to the films, while the main body of the bacteria is pushed away by repulsive forces, effectively anchoring it in place. The spread of EPS also changes the surface charges of $TiO_2$ as they interact, effectively neutralizing the electrostatic charges and changing interaction potentials. ROS effect of AgNP films does not consider the quenching mechanisms of EPS.

### 3.6. Microscopy analysis

$TiO_2$ thin films, used for experiments, were imaged using an optical microscope under bright-field conditions. As shown in **figure 18**, there are significant changes to the morphology of films.

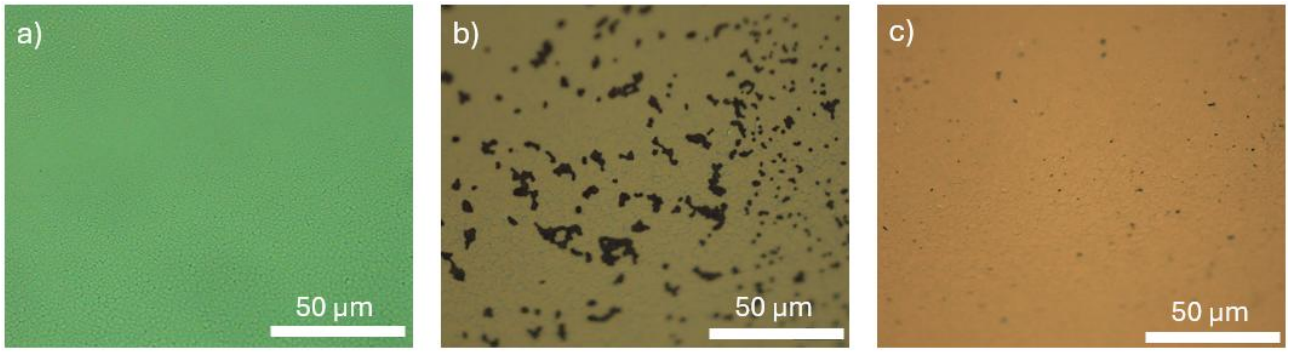


**Fig. 18**. Micrographs of $TiO_2$ films a) after deposition, b) post experiment and c) cleaned.

**Figure 18** illustrates the morphology changes of $TiO_2$ thin films at different stages of the experimental process. The films as-deposited show highly uniform, homogenous surface, without obvious defects. Following incubation with *Bacillus subtilis*, an alteration of the surface morphology is visible with clusters of round dots on the surface, indicative of *B. subtilis* spores. These spots highlight the adhesion interactions with the $TiO_2$ films, indicating high possibility of EPS compounds interacting with the film and anchoring the cells in place. After undergoing subsequent cleaning with distilled water and dried with high-pressure air, the adhered biomass is detached, leaving the films relatively clean, however, with some residual micro-specs. This could be due to spores being unable to repair the "glue" and release more EPS compounds.

Micrographs were taken of the AgNP-doped thin films post experiment as well, which is illustrated in **figure 19**.

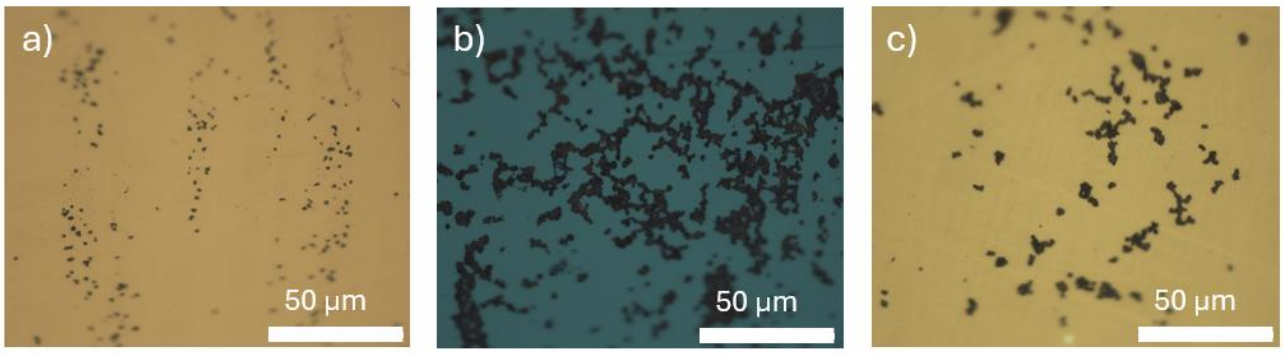


**Fig. 19.** Micrographs of AgNP+$TiO_2$ films at initial layer thicknesses of a) 5 nm, b) 7.5 nm and c) 10 nm post experiment.

The micrographs presented in **figure 19** are visual confirmation of the adhesion that could have caused the absence of colony-forming units (CFU) on agar plates. The standard wash protocols failed to overcome the primary energy minimum causing strong adhesion. The spatial distribution of the spores varies with film surface morphology, signifying that surface features such as surface roughness and distribution of AgNPs have an effect on the adhesion dynamics.

Cleaned and as-deposited AgNP doped films were imaged using dark-field microscopy to see the influence of experimental methodology on the film structure.

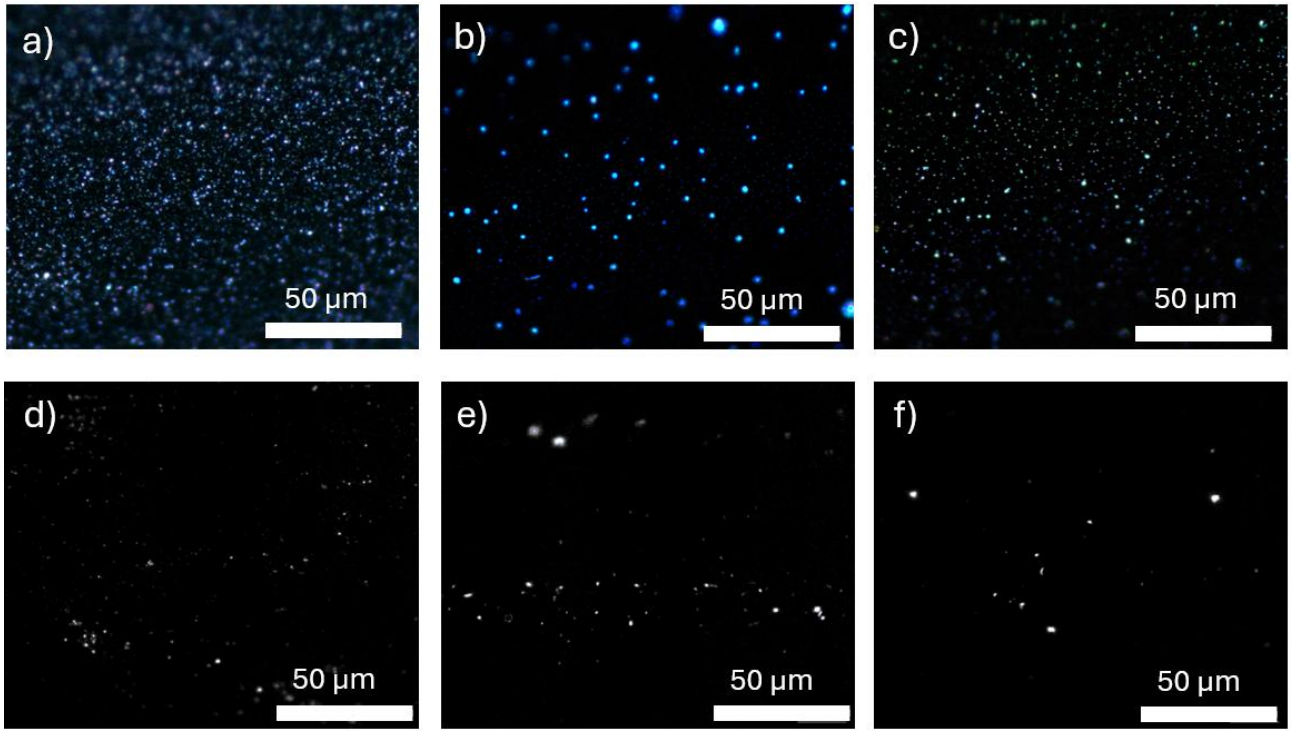


**Fig. 20.** Micrographs of AgNP+$TiO_2$ films after deposition (a-c) and after cleaning (d-f) with initial Ag layer thickness of 5 nm (a, d), 7.5 nm (b, e) and 10 nm (c, f).

As illustrated in **figure 20**, there are significant changes to the surface of the doped films. The films after deposition (a-c) show assumed agglomeration of nanoparticles across the surface, however, after cleaning, there is a reduction of these surface patterns visible in all samples (d-f). Comparatively, dark field microscopy of pure $TiO_2$ showed no surface patterns at all, hence why they were not included in the result section. Compositional analysis was not done to confirm the presence of AgNPs and the micrographs could potentially show Ag agglomerates or clusters, however, the reduction is noticeable either way. This shows that during the process of washing and cleaning, the AgNPs or Ag clusters come off of the films into the washing liquid. This could mean that the forces required to clean off the biomass off the films are enough to damage the structural integrity and cause the films to lose their initial antibacterial effect. The nanoparticles could have ended up in the post-washing bacterial suspension, which was plated on agar, causing further damage by releasing $Ag^+$ ions and resulting in no growth after incubation.

### 3.7. Discussion of results

The findings of this work reveal that the issue of experiment methodology does not stem from total bacterial eradication across all conditions, but rather from irreversible thermodynamic adhesion. The superhydrophilicity of the initial post-deposition thin films, coupled with rigid, stress-induced expression of extracellular polymeric substances (EPS) by *B. subtilis*, shifted the interaction system into the primary energy minimum, which induces irreversible adhesion. Standard washout protocols using saline or 1/500 nutrient broth (NB) failed to overcome these forces, leaving the spores attached to the surface of the substrate.

Research by Li *et al*. (2026) on the adherence property of EPS compounds indicated that the adherence of these compounds to surfaces is highly dependent on pH, oxygen content

and the hydrophilicity of the substrate [101]. A lower pH (pH = 4) and higher hydrophilicity induce stronger adhesive properties of EPS, which would explain the adherence of bacteria on the films used in this work. The stress-induced production of EPS by *B. subtilis* coupled with the generation of ROS by $TiO_2$ films, lowering the level of oxygen in the environment, enabled the bacteria to counteract the electrostatic repulsion properties of AgNP+$TiO_2$ thin films [101].

As the water contact angle measurements showed, the films used for the experiment are highly hydrophilic, which would cause the EPS to strongly bound to the surface of the thin films. While studies done by Mu *et al*. (2023), showcase the stronger adherence properties of Gram-negative and Gram-positive bacteria to hydrophobic and rougher surfaces, it also does not account for the interaction of biofilm compounds [102]. These various amino acids, ionizable functional groups and structural organization of EPS have a direct influence on increasing adherence to hydrophobic and hydrophilic surfaces, which is likely to be a contributing factor as to the reasons behind the results of this study [101]. The additional generated $H_2$ during photocatalysis could have also shifted the zeta potential of the $TiO_2$ to a positive value, which in turn caused increased adherence, as was described by studies done by Richtowsky *et al*. (2024), as bacteria are negatively charged [103]. These biological factors and potential changes were not taken into consideration when modelling interaction potential using XDLVO theory, which explains the differing results from the experimental section.

Micrographs taken of the films after washing, showed that the AgNPs or Ag clusters got washed off of the films, which poses a concern for the safety of using the films as surface coatings for medical applications. There is a risk involved in utilizing AgNPs for medical applications, especially where it is directly in contact with healthy human cells, not only bacteria. High uptake of AgNPs or $Ag^+$ can exhibit cytotoxicity to all cells in contact, especially if they come off of the surface coating [63]. The adherence and imbedding of AgNPs has to be secure to not introduce particular debris into the body. Compositional or surface analysis should be done to ensure that AgNPs are formed on the surface.

Further investigation is needed to find the dependency between the biological factors of bacteria and adherence to antibacterial surface coatings. Modifications to the antibacterial efficacy testing methods should include a wider range of variables that would help determine interactions more probable in real life applications. Modelling of bacterial and films interactions should include more biological variables, such as movement of the microorganisms, the potential ion, produced by bacteria or on the surface of EPS, interactions.

## Conclusions

1. XDLVO simulations demonstrated $TiO_2$ and AgNP/$TiO_2$ film interactions with *B. subtilis* bacteria. Investigations with $TiO_2$ showed that anatase remains inert under both dark and UV conditions, while AgNP/$TiO_2$ films showed a reduction in the bacterial population based on concentration. Reduction was accelerated under UV irradiation with increasing silver concentration due to generation of ROS and $Ag^+$ release. The simulation failed to consider biological factors of bacterial interactions, that overpower electrostatic interactions of $TiO_2$ thin films.

2. Validation of the modified ISO 27447:2019 experimental protocol revealed that current methodology for antibacterial efficiency testing does not take into consideration the production of EPS by *B. subtilis* under stress. Both saline and 1/500 NB wash protocols lacked the mechanical and chemical force required to overcome the adhesion of bacterial biofilms, causing bacteria to not be recovered for plating.

3. Water contact angle measurements revealed highly hydrophilic films, from baseline 57.44° ($TiO_2$) to approximately 1° (10 nm Ag). Bright-field and dark-field microscopy confirmed the degradation of AgNP/$TiO_2$ film surface morphology post-experimentation. As-deposited films exhibited highly uniform nanoparticles or cluster agglomeration, while cleaned AgNP/$TiO_2$ films revealed negligible silver content. Mechanical forces required to detach EPS compounds compromise structural integrity, potentially leading to release of cytotoxic $Ag^+$ ions into post-wash bacterial suspension.

## List of references


1. GHAVIDEL-SARDSAHRA, Amirhossein, FATTAHPOUR MARANDI, Mohammadtaghi, SEIFI, Arash, AFHAMI, Shirin, MONTAZERI, Mahnaz and YEKANINEJAD, Mir Saeed. Assessment of awareness, adherence, and barriers to device-associated infection prevention measures in intensive care units: A multi-center cross-sectional study. *American Journal of Infection Control*. February 2026. P. S0196655326001008.

2. JOHN, Innocent P., STEPHANO, Mussa A. and MAYENGO, Maranya M. Control strategies for the dynamics of catheter-associated urinary tract infection. *Scientific African*. March 2026. Vol. 31, p. e03271.

3. KHAN, Inam Danish, BASU, Atoshi, KIRAN, Sheshadri, TRIVEDI, Shaleen, PANDIT, Priyanka and CHATTORAJ, Anupam. Device-Associated Healthcare-Associated Infections (DA-HAI) and the caveat of multiresistance in a multidisciplinary intensive care unit. *Medical Journal Armed Forces India*. July 2017. Vol. 73, no. 3, p. 222–231.

4. MAKI, Gina and ZERVOS, Marcus. Health Care–Acquired Infections in Low- and Middle-Income Countries and the Role of Infection Prevention and Control. *Infectious Disease Clinics of North America*. September 2021. Vol. 35, no. 3, p. 827–839.

5. HORAN, Seamus, LEUNG, Vivian K.Y., KINSELLA, Paul M., FRIEDMAN, N. Deborah, THEVARAJAN, Irani and MARSHALL, Caroline. Comparison of coding data with clinical diagnosis of antibiotic-resistant healthcare-associated infections. *Infection, Disease & Health*. June 2026. Vol. 31, no. 2, p. 100405.

6. GINGICHASHVILI, Sarah, DUANIS-ASSAF, Danielle, SHEMESH, Moshe, FEATHERSTONE, John D. B., FEUERSTEIN, Osnat and STEINBERG, Doron. Bacillus subtilis Biofilm Development – A Computerized Study of Morphology and Kinetics. *Frontiers in Microbiology*. 7 November 2017. Vol. 8, p. 2072.

7. ADOCHIȚE, Cristina-Ș., VIȚELARU, Cătălin, PARAU, Anca C., KISS, Adrian E., PANĂ, Iulian, VLĂDESCU, Alina, COSTINAȘ, Sarah, MOGA, Marius, MUNTEAN, Radu, BADEA, Mihaela and IDOMIR, Mihaela. Synthesis and Investigation of Antibacterial Activity of Thin Films Based on TiO2-Ag and SiO2-Ag with Potential Applications in Medical Environment. *Nanomaterials*. 9 March 2022. Vol. 12, no. 6, p. 902.

8. JOLIVET, Aline, LABBÉ, Christophe, FRILAY, Cédric, DEBIEU, Olivier, MARIE, Philippe, HORCHOLLE, Bryan, LEMARIÉ, Franck, PORTIER, Xavier, GRYGIEL, Clara, DUPREY, Sylvain, JADWISIENCZAK, Wojciech, INGRAM, David, UPADHYAY, Mudit, DAVID, Adrian, FOUCHET, Arnaud, LÜDERS, Ulrike and CARDIN, Julien. Structural, optical, and electrical properties of TiO2 thin films deposited by ALD: Impact of the substrate, the deposited thickness and the deposition temperature. *Applied Surface Science*. January 2023. Vol. 608, p. 155214.

9. KHAN, Haritham, CHARLES, Hazina and LEE, Caroline Sunyong. Fabrication of noble-metal-free copper-doped TiO2 nanofibers synergized with acetic acid-treated g-C3N4 nanosheets for enhanced photocatalytic hydrogen evolution. *Applied Surface Science*. January 2023. Vol. 607, p. 155068.

10. KANG, Manil, KIM, Sok Won and PARK, Hyo Yeol. Optical properties of TiO2 thin films with crystal structure. *Journal of Physics and Chemistry of Solids*. December 2018. Vol. 123, p. 266–270.

11. JEEPA, K.J., RAJEESH, J., SUBASH, T.D., GAYATHRE LAKSHMI, M.A., ACCHUTHARAMAN, K.R., SENTHIL PANDIAN, M., ISMAIL FATHIMA, M. and SUBHA, T.D. Magnesium-doped TiO2 for economical perovskite solar cells. *Ceramics International*. November 2025. Vol. 51, no. 26, p. 49285–49294.

12. CABEZUELO, Oscar, PONCE-GONZALEZ, Luis N., MARIN, M. Luisa and BOSCA, Francisco. A highly efficient supported TiO2 photocatalyst for wastewater remediation in continuous flow. *Applied Materials Today*. December 2023. Vol. 35, p. 101947.

13. SAEEDI, Seyedeh Narges, RASOULIFARD, Mohammad Hossein, DORRAJI, Mir Saeed Seyed, DOUROUDGARI, Hamed and SEHATI, Negar. Enhanced photocatalytic degradation of organic pollutants using a TiO2–clay nanocomposite in a rotary photoreactor with experimental and theoretical insights. *Scientific Reports*. 31 October 2025. Vol. 15, no. 1, p. 38193.

14. FUJISHIMA, Akira and HONDA, Kenichi. Electrochemical Photolysis of Water at a Semiconductor Electrode. *Nature*. July 1972. Vol. 238, no. 5358, p. 37–38.

15. RAFIQUE, Muhammad, HAJRA, Syeda, IRSHAD, Muneeb, USMAN, Muhammad, IMRAN, Muhammad, ASSIRI, Mohammad A. and ASHRAF, Waqar Muhammad. Hydrogen Production Using $TiO_2$ -Based Photocatalysts: A Comprehensive Review. *ACS Omega*. 25 July 2023. Vol. 8, no. 29, p. 25640–25648.

16. LUKONG, V.T., UKOBA, K., YORO, K.O. and JEN, T.C. Annealing temperature variation and its influence on the self-cleaning properties of TiO2 thin films. *Heliyon*. May 2022. Vol. 8, no. 5, p. e09460.

17. BAKBOLAT, Baglan, DAULBAYEV, Chingis, SULTANOV, Fail, BEISSENOV, Renat, UMIRZAKOV, Arman, MEREKE, Almaz, BEKBAEV, Askhat and CHUPRAKOV, Igor. Recent Developments of TiO2-Based Photocatalysis in the Hydrogen Evolution and Photodegradation: A Review. *Nanomaterials*. 9 September 2020. Vol. 10, no. 9, p. 1790.

18. YAGHOUBI, Houman, TAGHAVINIA, Nima and ALAMDARI, Eskandar Keshavarz. Self cleaning TiO2 coating on polycarbonate: Surface treatment, photocatalytic and nanomechanical properties. *Surface and Coatings Technology*. January 2010. Vol. 204, no. 9–10, p. 1562–1568.

19. PAKDEL, Esfandiar, FAN, Suju, CHEN, Jianming and WANG, Xungai. Antibacterial wool fabric with enhanced photostability, UV protection and hydrophilicity through surface acylation and TiO2 nanocoating. *Applied Surface Science Advances*. September 2025. Vol. 29, p. 100814.

20. WANG, Heng, WANG, Yuting, LI, Chuang and JIA, Li. Fabrication of eco-friendly calcium crosslinked alginate electrospun nanofibres for rapid and efficient removal of Cu(II). *International Journal of Biological Macromolecules*. October 2022. Vol. 219, p. 1–10.

21. SADIA, Sumaiya Islam, SHISHIR, Md. Khalid Hossain, AHMED, Shanawaz, AIDID, Allah Rakha, ISLAM, Md. Mynul, RANA, Md. Masud, AL-REZA, Sharif Md. and ALAM, Md. Ashraful. Crystallographic biography on nanocrystalline phase of polymorphs titanium dioxide (TiO2): A perspective static review. *South African Journal of Chemical Engineering*. October 2024. Vol. 50, p. 51–64.

22. ANSARI, Fatemeh Sheikh and DANESHJOU, Sara. Optimizing the green synthesis of antibacterial TiO2 - anatase phase nanoparticles derived from spinach leaf extract. *Scientific Reports*. 28 September 2024. Vol. 14, no. 1, p. 22440.

23. XU, Wenwen, YANG, Wangjin, HAN, Chong, YANG, He and XUE, Xiangxin. Significant influences of TiO2 crystal structures on NO2 and HONO emissions from the nitrates photolysis. *Journal of Environmental Sciences*. April 2021. Vol. 102, p. 198–206.

24. LINSEBIGLER, Amy L., LU, Guangquan and YATES, John T. Photocatalysis on TiO2 Surfaces: Principles, Mechanisms, and Selected Results. *Chemical Reviews*. May 1995. Vol. 95, no. 3, p. 735–758.

25. SCARPELLI, Francesca, MASTROPIETRO, Teresa F., POERIO, Teresa and GODBERT, Nicolas. Mesoporous TiO2 Thin Films: State of the Art. In : YANG, Dongfang (ed.), *Titanium Dioxide - Material for a Sustainable Environment*. Online. InTech, 2018. [Accessed 18 May 2026]. ISBN 978-1-78923-326-1.

26. BIRSAN, Iulian-Gabriel, PINTILIE, Stefan Catalin, PINTILIE, Laurentia Geanina, LAZAR, Andreea Liliana, CIRCIUMARU, Adrian and BALTA, Stefan. New Understanding of the Difference in Filtration Performance between Anatase and Rutile TiO2 Nanoparticles through Blending into Ultrafiltration PSF Membranes. *Membranes*. 29 October 2021. Vol. 11, no. 11, p. 841.

27. SEREMAK, Wioletta, BASZCZUK, Agnieszka, JASIORSKI, Marek, GIBAS, Anna and WINNICKI, Marcin. Photocatalytic Activity Enhancement of Low-pressure Cold-Sprayed TiO2 Coatings Induced by Long-term Water Vapor Exposure. *Journal of Thermal Spray Technology*. October 2021. Vol. 30, no. 7, p. 1827–1836.

28. KARUNADASA, Kohobhange S.P. and MANORATNE, C.H. Microstructural view of anatase to rutile phase transformation examined by in-situ high-temperature X-ray powder diffraction. *Journal of Solid State Chemistry*. October 2022. Vol. 314, p. 123377.

29. LI, Zhuoqing, LI, Li'ang, SOKOLOVA, Inna, SHANG, Yueyong, HUANG, Wei, KHOR, Waiho, FANG, James K.H., WANG, Youji and HU, Menghong. Effects of elevated temperature and different crystal structures of TiO2 nanoparticles on the gut microbiota of mussel Mytilus coruscus. *Marine Pollution Bulletin*. February 2024. Vol. 199, p. 115979.

30. DURANTE, Ofelia, GRANATA, Veronica, FITTIPALDI, Rosalba, NEILSON, Joshua, CARAPELLA, Giovanni, CHIADINI, Francesco, DESALVO, Riccardo, DE SIMONE, Roberta, DINELLI, Franco, FIUMARA, Vincenzo, PIERRO, Vincenzo, PINTO, Innocenzo Mario, VECCHIONE, Antonio, BOBBA, Fabrizio and DI GIORGIO, Cinzia. Role of oxygen vacancies in the structural phase transformations of granular TiO2 thin films. *Surfaces and Interfaces*. April 2023. Vol. 37, p. 102698.

31. ZHANG, Pingli, WANG, Chongyi and YU, Dongxue. Hot electron transfer induced by surface Plasmon in Ag/TiO2 system. *Thin Solid Films*. August 2024. Vol. 803, p. 140470.

32. MUTHEE, Dorah Kawira, DEJENE, Francis Birhanu and MUNGUTI, Lawrence Kioko. Modification of TiO2 anatase-rutile mixed-phase properties using Sn4+ doping for photocatalytic brilliant green degradation. *Applied Catalysis A: General*. April 2025. Vol. 695, p. 120166.

33. SUJATHA, Gurudev, SHANTHAKUMAR, Subramaniam and CHIAMPO, Fulvia. UV Light-Irradiated Photocatalytic Degradation of Coffee Processing Wastewater Using TiO2 as a Catalyst. *Environments*. 19 June 2020. Vol. 7, no. 6, p. 47.

34. LIANG, Shuang, ZENG, Yuan, JING, Jiana and SUN, Zhirong. Tuning surface defects of B-doped TiO2 for efficient ceftazidime photodegradation: The role of electronic structure in molecular oxygen activation and superoxide radical utilization. *Applied Surface Science*. June 2026. Vol. 732, p. 166496.

35. RAJENDRAN, Swarna Lakshmi and ALAGAN, Viswanathan. One-dimensional titanium dioxide nanotube arrays for hydrogen generation. *Journal of Chemical Sciences*. 12 September 2025. Vol. 137, no. 4, p. 79.

36. HONG, Yuzhi, ZENG, Jie, WANG, Xiuhong, DRLICA, Karl and ZHAO, Xilin. Post-stress bacterial cell death mediated by reactive oxygen species. *Proceedings of the National Academy of Sciences*. 14 May 2019. Vol. 116, no. 20, p. 10064–10071.

37. YOU, Dong Gil, DEEPAGAN, V. G., UM, Wooram, JEON, Sangmin, SON, Sejin, CHANG, Hyeyoun, YOON, Hwa In, CHO, Yong Woo, SWIERCZEWSKA, Maggie, LEE, Seulki, POMPER, Martin G., KWON, Ick Chan, KIM, Kwangmeyung and PARK, Jae Hyung. ROS-generating TiO2 nanoparticles for non-invasive sonodynamic therapy of cancer. *Scientific Reports*. 21 March 2016. Vol. 6, no. 1, p. 23200.

38. KUJAWA, Weronika, DIDYK-MUCHA, Agnieszka, OLEWNIK-KRUSZKOWSKA, Ewa, GIERSZEWSKA, Magdalena and RUDAWSKA, Anna. Synergistic Effect of Combined Polymorphs Anatase-Rutile Nano-Modified Lightweight Concrete on Photocatalytic Reduction of NOx, Self-Cleaning Performance, and Antimicrobial Properties. *Buildings*. 8 July 2023. Vol. 13, no. 7, p. 1736.

39. KIM, Min Gu, KANG, Jeong Min, LEE, Ji Eun, KIM, Kang Seok, KIM, Kwang Ho, CHO, Min and LEE, Seung Geol. Effects of Calcination Temperature on the Phase Composition, Photocatalytic Degradation, and Virucidal Activities of $TiO_2$ Nanoparticles. *ACS Omega*. 27 April 2021. Vol. 6, no. 16, p. 10668–10678.

40. DA SILVA, Elisangela P., WINKLER, Manuel E.G., GIUFRIDA, Willyan M., CARDOZO-FILHO, Lucio, ALONSO, Christian G., LOPES, Jardel B.O., RUBIRA, Adley F. and SILVA, Rafael. Effect of phase composition on the photocatalytic activity of titanium dioxide obtained from supercritical antisolvent. *Journal of Colloid and Interface Science*. February 2019. Vol. 535, p. 245–254.

41. BALAMURUGAN, M., SILAMBARASAN, M., SARAVANAN, S. and SOGA, T. Synthesis of anatase and rutile mixed phase titanium dioxide nanoparticles using simple solution combustion method. *Physica B: Condensed Matter*. August 2022. Vol. 638, p. 413843.

42. SHIM, Sunyong, UEDA, Kyosuke, OGASAWARA, Kouetsu and NARUSHIMA, Takayuki. Fabrication of N-doped TiO2 thin films by reactive sputtering: The key roles of phase and substitutional nitrogen on visible-light-induced photocatalytic and antibacterial activities. *Applied Surface Science Advances*. September 2026. Vol. 34, p. 100982.

43. RAHMI, HARNILA, LUBIS, Surya, JULINAWATI, MUSTAFA, Irfan and MZ, Kartika. Fabrication of Glycine-Chitosan/TiO2 film for metanil yellow removal from water. *South African Journal of Chemical Engineering*. January 2024. Vol. 47, p. 254–261.

44. KHLYUSTOVA, Anna, SIROTKIN, Nikolay, KUSOVA, Tatiana, KRAEV, Anton, TITOV, Valery and AGAFONOV, Alexander. Doped $TiO_2$: the effect of doping elements on photocatalytic activity. *Materials Advances*. 2020. Vol. 1, no. 5, p. 1193–1201.

45. RACOVITA, Anca Diana. Titanium Dioxide: Structure, Impact, and Toxicity. *International Journal of Environmental Research and Public Health*. 6 May 2022. Vol. 19, no. 9, p. 5681.

46. PARK, Byung-Geon. Photocatalytic Activity of TiO2-Doped Fe, Ag, and Ni with N under Visible Light Irradiation. *Gels*. 24 December 2021. Vol. 8, no. 1, p. 14.

47. MUTHUKRISHNAN, S., VIDYA, R. and SJÅSTAD, Anja Olafsen. Band gap engineering of anatase TiO2 by ambipolar doping: A first principles study. *Materials Chemistry and Physics*. April 2023. Vol. 299, p. 127467.

48. RIBAO, Paula, RIVERO, Maria J. and ORTIZ, Inmaculada. TiO2 structures doped with noble metals and/or graphene oxide to improve the photocatalytic degradation of dichloroacetic acid. *Environmental Science and Pollution Research*. May 2017. Vol. 24, no. 14, p. 12628–12637.

49. YERGALIYEVA, S., NEMKAYEVA, R., GUSEINOV, N., PRIKHODKO, O., ARBUZ, A., ORYNBAY, B., SAGIDOLDA, Ye., AITZHANOV, M., ISMAILOVA, G. and MUKHAMETKARIMOV, Y. Synthesis and optical properties of Ag/Au-$TiO_2$ plasmonic composite thin films. *Optical Materials Express*. 1 October 2023. Vol. 13, no. 10, p. 2726.

50. ALZOUBI, F. Y., AHMAD, Ahmad A., ALJARRAH, Ihsan A., MIGDADI, A. B. and AL-BATAINEH, Qais M. Localize surface plasmon resonance of silver nanoparticles using Mie theory. *Journal of Materials Science: Materials in Electronics*. November 2023. Vol. 34, no. 32, p. 2128.

51. SOLDO-OLIVIER, Y., ABISSET, A., BAILLY, A., DE SANTIS, M., GARAUDÉE, S., LACIPIÈRE, J., COATI, A., GARREAU, Y. and SAINT-LAGER, M.-C. Localized surface plasmon resonance of Au/$TiO_2$ (110): substrate and size influence from *in situ* optical and structural investigation. *Nanoscale Advances*. 2020. Vol. 2, no. 6, p. 2448–2461.

52. KAVALIŪNAS, Vytautas, ČEPLIKAS, Paulius, SRIUBAS, Mantas and LAUKAITIS, Giedrius. The Sensitization of TiO2 Thin Film by Ag Nanoparticles for the Improvement of Photocatalytic Efficiency. *Applied Sciences*. 4 June 2022. Vol. 12, no. 11, p. 5725.

53. CAI, Peng-Fei, LI, Jun, WU, Xin-Bao, LI, Zhao-Yang, SHEN, Jie, NIE, Jing-Jun, CUI, Zhen-Duo, CHEN, Da-Fu, LIANG, Yan-Qin, ZHU, Sheng-Li and WU, Shui-Lin. ALD-induced $TiO_2$ /Ag nanofilm for rapid surface photodynamic ion sterilization. *Rare Metals*. December 2022. Vol. 41, no. 12, p. 4138–4148.

54. BHUSKUTE, Bela D., TINUS, Tuomas, ALI-LÖYTTY, Harri, SAARI, Jesse, LAHTONEN, Kimmo and VALDEN, Mika. Low-density Ag–Au nanoparticle photodeposition on $TiO_2$ thin film photocatalysts grown by atomic layer deposition. *Physical Chemistry Chemical Physics*. 2025. Vol. 27, no. 32, p. 16865–16874.

55. BORREGO PÉREZ, J.A., MORALES, E.R., PARAGUAY DELGADO, F., MEZA AVENDAÑO, C.A., ALONSO GUZMAN, E.M. and MATHEWS, N.R. Ag nanoparticle dispersed TiO2 thin films by single step sol gel process: Evaluation of the physical properties and photocatalytic degradation. *Vacuum*. September 2023. Vol. 215, p. 112276.

56. KONEV, D, KAZAKIN, A, VOROBYEV, A, ENNS, Y, KUZNETSOV, A, KONDRATEVA, A and MISHIN, M. Magnetron sputtered $TiO_2$ with metal NPs for plasmonic applications. *Journal of Physics: Conference Series*. 1 December 2021. Vol. 2086, no. 1, p. 012018.

57. ASHOK, Allamula, KARAN, Vir, LASYA, Peela, JACOB, Daljin, SWAMINATHAN, Parasuraman and YADAV, Satyesh Kumar. Optimization of the Deposition Process Parameters of DC Magnetron Sputtering to Achieve Desired Deposition Rate Using Design of Experiment Method. *Journal of Electronic Materials*. October 2023. Vol. 52, no. 10, p. 6851–6863.

58. SUN, Li, QUE, Zhuoqun, RUAN, Ting, YUAN, Zhigang, GONG, Wenbang, MEI, Shunqi, CHEN, Zhen and LIU, Ying. The Synthesis of Ag/TiO2 via the DC Magnetron Sputtering Method and Its Application in the Photocatalytic Degradation of Methyl Orange in Na2SO4 Solution. *Applied Sciences*. 9 May 2024. Vol. 14, no. 10, p. 4014.

59. POKORNÝ, P., MUSIL, J., LANČOK, J., FITL, P., NOVOTNÝ, M., BULÍŘ, J. and VLČEK, J. Mass spectrometry investigation of magnetron sputtering discharges. *Vacuum*. September 2017. Vol. 143, p. 438–443.

60. JANG, Gil Su, AHN, Seon Mi and HWANG, Nong-Moon. Effects of Sputtering Power, Working Pressure, and Electric Bias on the Deposition Behavior of Ag Films during DC Magnetron Sputtering Considering the Generation of Charged Flux. *Electronic Materials Letters*. January 2022. Vol. 18, no. 1, p. 57–68.

61. LEE, Taeho, PARK, Jin-Seok and OH, Saeroonter. Effect of sputtering working pressure on the reliability and performance of amorphous indium gallium zinc oxide thin film transistors. *AIP Advances*. 1 March 2024. Vol. 14, no. 3, p. 035145.

62. GRISHIN, T.S., VOLKOVA, L.S., DUDIN, A.A., MEDENKOV, G.A., NOVIKOV, D.V., DUBKOV, S.V. and GROMOV, D.G. Evolution of morphological parameters in self-assembled Ag nanoparticle arrays for high-performance SERS. *Optical Materials*. October 2025. Vol. 167, p. 117260.

63. BARBALINARDO, Marianna, BENVENUTI, Emilia, GENTILI, Denis, CHIARINI, Francesca, BERTACCHINI, Jessika, RONCUCCI, Luca and SENA, Paola. Differential Cytotoxicity of Surface-Functionalized Silver Nanoparticles in Colorectal Cancer and Ex-Vivo Healthy Colonocyte Models. *Cancers*. 27 April 2025. Vol. 17, no. 9, p. 1475.

64. TSAI, Yu Hsin, KUMARIHAMY, Maheshika, PONCE, Nicole Beatrice, ALAM, Md. Masud, KIM, Wooram, YU, Xiong, KIM, Tae Kyong John and SAMIA, Anna Cristina S. Tailored $TiO_2$ Nanoparticles for Broad-Spectrum Antibiofilm Applications: A Systematic Comparison of Structural and Functional Properties of Carbon- and Nitrogen-Doped $TiO_2$ Nanoparticles. *ACS Applied Engineering Materials*. 27 February 2026. Vol. 4, no. 2, p. 882–896.

65. JALALI, S.A.H., ALLAFCHIAN, A.R., BANIFATEMI, S.S. and ASHRAFI TAMAI, I. The antibacterial properties of Ag/TiO 2 nanoparticles embedded in silane sol–gel matrix. *Journal of the Taiwan Institute of Chemical Engineers*. September 2016. Vol. 66, p. 357–362.

66. PETCU, Ionela-Cristina, NEGREA, Raluca, BRANDÃO, Ana T.S.C., ROMANITAN, Cosmin, BRINCOVEANU, Oana, DJOURELOV, Nikolay, MIHALACHE, Iuliana, VECA, L. Monica, ISOPENCU, Gabriela, PEREIRA, Carlos M., ANICAI, Liana, BUSUIOC, Cristina and (ROSOIU), Sabrina State. Pulsed reverse electrochemical synthesis of Ag-TiO2

composites from deep eutectic solvents: Photocatalytic and antibacterial behaviour. *Applied Surface Science Advances*. June 2025. Vol. 27, p. 100749.

67. MAFHALA, Livhuwani, KHUMALO, Nomcebo, ZIKALALA, Nkosingiphile Excellent, AZIZI, Shohreh, CLOETE, Karen Jacqueline, MORE, Garland Kgosi, KAMIKA, Ilunga Alain, MOKRANI, Touhami, ZINATIZADEH, Ali Akbar and MAAZA, Malik. Antibacterial and cytotoxicity activity of green synthesized silver nanoparticles using aqueous extract of naartjie (Citrus unshiu) fruit peels. *Emerging Contaminants*. December 2024. Vol. 10, no. 4, p. 100348.

68. ZHANG, Qingbo, HU, Yue, MASTERSON, Caitlin M., JANG, Wonhee, XIAO, Zhen, BOHLOUL, Arash, GARCIA-ROJAS, Daniel, PUPPALA, Hema L., BENNETT, George and COLVIN, Vicki L. When function is biological: Discerning how silver nanoparticle structure dictates antimicrobial activity. *iScience*. July 2022. Vol. 25, no. 7, p. 104475.

69. RAHMATPOUR, Samaneh, SHIRVANI, Mehran, MOSADDEGHI, Mohammad R., NOURBAKHSH, Farshid and BAZARGANIPOUR, Mehdi. Dose–response effects of silver nanoparticles and silver nitrate on microbial and enzyme activities in calcareous soils. *Geoderma*. January 2017. Vol. 285, p. 313–322.

70. JAHAN, Israt, MATPAN BEKLER, Fatma, TUNÇ, Ahmed and GÜVEN, Kemal. The Effects of Silver Nanoparticles (AgNPs) on Thermophilic Bacteria: Antibacterial, Morphological, Physiological and Biochemical Investigations. *Microorganisms*. 17 February 2024. Vol. 12, no. 2, p. 402.

71. FERNANDES, Mário, GONZÁLEZ-BALLESTEROS, Noelia, DA COSTA, André, MACHADO, Raúl, GOMES, Andreia C. and RODRÍGUEZ-ARGÜELLES, Maria Carmen. Antimicrobial and anti-biofilm activity of silver nanoparticles biosynthesized with Cystoseira algae extracts. *JBIC Journal of Biological Inorganic Chemistry*. 21 April 2023. Vol. 28, no. 4, p. 439–450.

72. YELEMANE, Vikas, KANGWA, Martin, DSOUZA, Roy N. and FERNÁNDEZ-LAHORE, Marcelo. Surface energetics to assess influence of biomass-type and biomass–adsorbent interactions in expanded beds. *Bioresources and Bioprocessing*. 13 April 2021. Vol. 8, no. 1, p. 29.

73. ZHAO, Dan, LOUISE LETH, Maria, ABOU HACHEM, Maher, AZIZ, Iram, JANČIČ, Natalija, LUXBACHER, Thomas, HÉLIX-NIELSEN, Claus and ZHANG, Wenjing. Facile fabrication of flexible ceramic nanofibrous membranes for enzyme immobilization and transformation of emerging pollutants. *Chemical Engineering Journal*. January 2023. Vol. 451, p. 138902.

74. FENG, Xiao-Chi, GUO, Wan-Qian, ZHENG, He-Shan, WU, Qing-Lian, LUO, Hai-Chao and REN, Nan-Qi. Effect of metabolic uncoupler, 3,3′,4′,5-tetrachlorosalicylanilide (TCS) on *Bacillus subtilis* : biofilm formation, flocculability and surface characteristics. *RSC Advances*. 2018. Vol. 8, no. 29, p. 16178–16186.

75. LI, Yuanzhe, LI, Xiang, HAO, Yu, LIU, Yang, DONG, ZhiLi and LI, Kexin. Biological and Physiochemical Methods of Biofilm Adhesion Resistance Control of Medical-Context Surface. *International Journal of Biological Sciences*. 2021. Vol. 17, no. 7, p. 1769–1781.

76. BILEK, Ondrej, FIALOVA, Tatiana, OTAHAL, Alexandr, ADAM, Vojtech, SMERKOVA, Kristyna and FOHLEROVA, Zdenka. Antibacterial activity of AgNPs–$TiO_2$ nanotubes:

influence of different nanoparticle stabilizers. *RSC Advances*. 2020. Vol. 10, no. 72, p. 44601–44610.

77. KOZAK, Magda, MAZIERSKI, Paweł, ŻEBROWSKA, Joanna, KLIMCZUK, Tomasz, LISOWSKI, Wojciech, ŻAK, Andrzej M., SKOWRON, Piotr M. and ZALESKA-MEDYNSKA, Adriana. Detailed Insight into Photocatalytic Inactivation of Pathogenic Bacteria in the Presence of Visible-Light-Active Multicomponent Photocatalysts. *Nanomaterials*. 23 February 2024. Vol. 14, no. 5, p. 409.

78. EL-KHAWAGA, Ahmed M., AYMAN, Mohamed, HAFEZ, Omar and SHALABY, Rasha E. Photocatalytic, antimicrobial and antibiofilm activities of MgFe2O4 magnetic nanoparticles. *Scientific Reports*. 5 June 2024. Vol. 14, no. 1, p. 12877.

79. ZHANG, Chi, LI, Yi, WANG, Chao and ZHENG, Xinyi. Different inactivation behaviors and mechanisms of representative pathogens (Escherichia coli bacteria, human adenoviruses and Bacillus subtilis spores) in g-C3N4-based metal-free visible-light-enabled photocatalytic disinfection. *Science of The Total Environment*. February 2021. Vol. 755, p. 142588.

80. LIU, Yanfeng, SU, Anqi, TIAN, Rongzhen, LI, Jianghua, LIU, Long and DU, Guocheng. Developing rapid growing Bacillus subtilis for improved biochemical and recombinant protein production. *Metabolic Engineering Communications*. December 2020. Vol. 11, p. e00141.

81. GINGICHASHVILI, Sarah, DUANIS-ASSAF, Danielle, SHEMESH, Moshe, FEATHERSTONE, John D. B., FEUERSTEIN, Osnat and STEINBERG, Doron. Bacillus subtilis Biofilm Development – A Computerized Study of Morphology and Kinetics. *Frontiers in Microbiology*. 7 November 2017. Vol. 8, p. 2072.

82. TIAN, Zhiliang, HOU, Lizhen, HU, Miao, GAO, Yaxin, LI, Danfeng, FAN, Bei, WANG, Fengzhong and LI, Shuying. Optimization of Sporulation Conditions for Bacillus subtilis BSNK-5. *Processes*. 6 June 2022. Vol. 10, no. 6, p. 1133.

83. MU, Haoyan, WANG, Yiheng, PEI, Yongfu, WANG, Xin, DAI, Xiongfeng and ZHU, Manlu. Condition-dependent resource allocation strategy governed by CodY regulator in *Bacillus subtilis*. *mLife*. October 2025. Vol. 4, no. 5, p. 539–550.

84. BILLAUDEAU, Cyrille, CHASTANET, Arnaud, YAO, Zhizhong, CORNILLEAU, Charlène, MIROUZE, Nicolas, FROMION, Vincent and CARBALLIDO-LÓPEZ, Rut. Contrasting mechanisms of growth in two model rod-shaped bacteria. *Nature Communications*. 7 June 2017. Vol. 8, no. 1, p. 15370.

85. KEARNS, Daniel B. and LOSICK, Richard. Cell population heterogeneity during growth of *Bacillus subtilis*. *Genes & Development*. 15 December 2005. Vol. 19, no. 24, p. 3083–3094.

86. ERRINGTON, Jeff. Regulation of endospore formation in Bacillus subtilis. *Nature Reviews Microbiology*. November 2003. Vol. 1, no. 2, p. 117–126.

87. IWAŃSKA, Olga, LATOCH, Przemysław, KOPIK, Natalia, KOVALENKO, Mariia, LICHOCKA, Małgorzata, SERWA, Remigiusz and STAROSTA, Agata L. Translation in Bacillus subtilis is spatially and temporally coordinated during sporulation. *Nature Communications*. 21 August 2024. Vol. 15, no. 1, p. 7188.

88. SINGH, Shyam K., ALI, Mohamed Medhat, SAMARANAYAKE, Chaminda P., LIU, Huihong, SETLOW, Peter and SASTRY, Sudhir. Effect of electric field frequency on inactivation of the Bacillus subtilis spore and its mutants during ohmic heating. *Food and Bioproducts Processing*. July 2025. Vol. 152, p. 128–138.

89. SCHWARZENBERGER, Tim, SCHÖN, Karl-Heinz, EGGERS, Jutta, NEVAS, Saulius, SCHRÖPPEL, Felix, SCHWIND, Kerstin and SPERFELD, Peter. Action spectrum of Bacillus subtilis spores for validation of polychromatic ultraviolet (UV) systems. *Water Research*. December 2025. Vol. 287, p. 124329.

90. FENG, Xiao-Chi, GUO, Wan-Qian, ZHENG, He-Shan, WU, Qing-Lian, LUO, Hai-Chao and REN, Nan-Qi. Effect of metabolic uncoupler, 3,3′,4′,5-tetrachlorosalicylanilide (TCS) on *Bacillus subtilis* : biofilm formation, flocculability and surface characteristics. *RSC Advances*. 2018. Vol. 8, no. 29, p. 16178–16186.

91. HU, Ying, WANG, Jian, SUN, Hongwei, WANG, Shaohui, LIAO, Xiaomei, WANG, Jun and AN, Taicheng. Roles of extracellular polymeric substances in the bactericidal effect of nanoscale zero-valent iron: trade-offs between physical disruption and oxidative damage. *Environmental Science: Nano*. 2019. Vol. 6, no. 7, p. 2061–2073.

92. OLIVA, Rebeca Leme, KHADKA, Umesh B., CAMENZIND, Tessa, DYCKMANS, Jens and JOERGENSEN, Rainer Georg. Constituent of extracellular polymeric substances (EPS) produced by a range of soil bacteria and fungi. *BMC Microbiology*. 15 May 2025. Vol. 25, no. 1, p. 298.

93. PAJERSKI, Wojciech, OCHONSKA, Dorota, BRZYCHCZY-WLOCH, Monika, INDYKA, Paulina, JAROSZ, Magdalena, GOLDA-CEPA, Monika, SOJKA, Zbigniew and KOTARBA, Andrzej. Attachment efficiency of gold nanoparticles by Gram-positive and Gram-negative bacterial strains governed by surface charges. *Journal of Nanoparticle Research*. August 2019. Vol. 21, no. 8, p. 186.

94. INTERNATIONAL ORGANIZATION FOR STANDARDIZATION. ISO 27447:2019: *Fine ceramics (advanced ceramics, advanced technical ceramics) — Test method for antibacterial activity of semiconducting photocatalytic materials* Online. International Organization for Standardization, 2019. Available from: https://www.iso.org/standard/69874.html.

95. RAZAK, Kamrosni Abdul, HALIN, Dewi Suriyani Che, ABDULLAH, Mohd Mustafa Al Bakri, AZANI, Azliza, MOHD SALLEH, Mohd Arif Anuar, MAHMED, Norsuria and CHOBPATTANA, Varistha. Self - Cleaning Property of Ag/$TiO_2$ Thin Film. *Materials Science Forum*. 17 September 2020. Vol. 1010, p. 397–404.

96. NATH, Amitabha, SINGH, Laishram Robindro and SARKAR, Mitra Barun. Enhanced surface wettability of Ag:TiO2 heterostructured assembly using double step glancing angle deposition technique. *Ceramics International*. April 2022. Vol. 48, no. 8, p. 11392–11400.

97. STAMENKOVIĆ-STOJANOVIĆ, Sandra, KARABEGOVIĆ, Ivana, BEŠKOSKI, Vladimir, NIKOLIĆ, Nada and LAZIĆ, Miodrag. Bacillus subtilis NCIM2063 batch cultivation: The influence of the substrate concentration and oxygen transfer rate on the biomass yield. *Advanced Technologies*. 2020. Vol. 9, no. 1, p. 44–49.

98. SŁABICKA-JAKUBCZYK, Anna, LEWANDOWSKI, Miłosz, PASTUSZAK, Paulina, BARAŃSKA-RYBAK, Wioletta and GÓRSKA-PONIKOWSKA, Magdalena. Influence of UV

nail lamps radiation on human keratinocytes viability. *Scientific Reports*. 18 December 2023. Vol. 13, no. 1, p. 22530.

99. TAYLOR, Willie, CAMILLERI, Emily, CRAFT, D. Levi, KORZA, George, GRANADOS, Maria Rocha, PETERSON, Jaliyah, SZCZPANIAK, Renata, WELLER, Sandra K., MOELLER, Ralf, DOUKI, Thierry, MOK, Wendy W. K. and SETLOW, Peter. DNA Damage Kills Bacterial Spores and Cells Exposed to 222-Nanometer UV Radiation. SCHAFFNER, Donald W. (ed.), *Applied and Environmental Microbiology*. April 2020. Vol. 86, no. 8, p. e03039-19.

100. HANDLER, F.A. Predicting Inactivation of *Bacillus subtilis* Spores Exposed to Broadband and Solar Ultraviolet Light. *Environmental Engineering Science*. 1 June 2019. Vol. 36, no. 6, p. 667–680.

101. LI, Ji, HERMELIJN, Jeenah, VAN LOOSDRECHT, Mark C.M. and LIN, Yuemei. Adhesion and binding properties of extracellular polymeric substances (EPS) extracted from activated sludge. *Bioresource Technology*. July 2026. Vol. 451, p. 134544.

102. MU, Minchen, LIU, Shuhao, DEFLORIO, William, HAO, Li, WANG, Xunhao, SALAZAR, Karla Solis, TAYLOR, Matthew, CASTILLO, Alejandro, CISNEROS-ZEVALLOS, Luis, OH, Jun Kyun, MIN, Younjin and AKBULUT, Mustafa. Influence of Surface Roughness, Nanostructure, and Wetting on Bacterial Adhesion. *Langmuir*. 18 April 2023. Vol. 39, no. 15, p. 5426–5439.

103. RYCHTOWSKI, Piotr, PASZKIEWICZ, Oliwia, MARKOWSKA-SZCZUPAK, Agata, LENIEC, Grzegorz and TRYBA, Beata. Sulphated TiO2 Reduced by Ammonia and Hydrogen as an Excellent Photocatalyst for Bacteria Inactivation. *Materials*. 22 December 2023. Vol. 17, no. 1, p. 66.